NAVAL POSTGRADUATE SCHOOL

MONTEREY, CALIFORNIA

THESIS

PHOTOVOLTAIC ARRAY MAXIMUM POWER POINT TRACKING DIGITAL IMPLEMENTATION AND EFFICIENCY ANALYSIS

by

David B. Lorio

September 2020

Thesis Advisor: Giovanna Oriti
Co-Advisor: Di Zhang

THIS PAGE INTENTIONALLY LEFT BLANK

REPORT DOCUMENTATION PAGE			*Form Approved OMB No. 0704-0188*

1. AGENCY USE ONLY *(Leave blank)*	**2. REPORT DATE** September 2020	**3. REPORT TYPE AND DATES COVERED** Master's thesis

4. TITLE AND SUBTITLE PHOTOVOLTAIC ARRAY MAXIMUM POWER POINT TRACKING DIGITAL IMPLEMENTATION AND EFFICIENCY ANALYSIS	**5. FUNDING NUMBERS**
6. AUTHOR(S) David B. Lorio	
7. PERFORMING ORGANIZATION NAME(S) AND ADDRESS(ES) Naval Postgraduate School Monterey, CA 93943-5000	**8. PERFORMING ORGANIZATION REPORT NUMBER**
9. SPONSORING / MONITORING AGENCY NAME(S) AND ADDRESS(ES) N/A	**10. SPONSORING / MONITORING AGENCY REPORT NUMBER**

11. SUPPLEMENTARY NOTES The views expressed in this thesis are those of the author and do not reflect the official policy or position of the Department of Defense or the U.S. Government.

12a. DISTRIBUTION / AVAILABILITY STATEMENT Approved for public release. Distribution is unlimited.	**12b. DISTRIBUTION CODE** A

13. ABSTRACT (maximum 200 words)

The current United States Navy and Marine Corps warfighting concepts focus on distributed and decentralized operations to increase the lethality and security of the force as a whole. An amplified reliance on electrical energy to power weapon systems and the command and control structure, in conjunction with a dispersed force, escalates the logistical requirements for any unit. Renewable energy resources, such as solar radiation, may be a means of reducing this logistical burden; however, photovoltaic (PV) arrays must operate at their maximum power point for these systems to be more effective. This thesis studies the efficiencies of the controller for a PV power conditioning system implementing the two most common maximum power point tracking (MPPT) algorithms, "Perturb and Observe" and "Incremental Conductance." The system includes a commercial-off-the-shelf PV array, buck DC-DC converter, lead-acid batteries as its energy storage system and load, and an Opal-RT real-time simulator for rapid control prototyping. The efficiency of the MPPT controller was studied via simulation and improved through parameter optimization. The control algorithms were executed in a physical system using a hardware-in-the-loop testing configuration and the measured values were compared to the simulated results. Experimental testing confirmed the MPPT controller performed as designed and achieved the expected efficiency for the various solar irradiances and temperatures under which it was tested.

14. SUBJECT TERMS solar, photovoltaic, stand-alone PV system, buck converter, maximum power point tracking, MPPT, perturb and observe, incremental conductance, real-time simulation, Opal-RT	**15. NUMBER OF PAGES** 89
	16. PRICE CODE

17. SECURITY CLASSIFICATION OF REPORT	**18. SECURITY CLASSIFICATION OF THIS PAGE**	**19. SECURITY CLASSIFICATION OF ABSTRACT**	**20. LIMITATION OF ABSTRACT**
Unclassified	Unclassified	Unclassified	UU

NSN 7540-01-280-5500 Standard Form 298 (Rev. 2-89) Prescribed by ANSI Std. 239-18

THIS PAGE INTENTIONALLY LEFT BLANK

Approved for public release. Distribution is unlimited.

PHOTOVOLTAIC ARRAY MAXIMUM POWER POINT TRACKING DIGITAL IMPLEMENTATION AND EFFICIENCY ANALYSIS

David B. Lorio
Captain, United States Marine Corps
BS, U.S. Naval Academy, 2014

Submitted in partial fulfillment of the
requirements for the degree of

MASTER OF SCIENCE IN ELECTRICAL ENGINEERING

from the

NAVAL POSTGRADUATE SCHOOL
September 2020

Approved by: Giovanna Oriti
Advisor

Di Zhang
Co-Advisor

Douglas J. Fouts
Chair, Department of Electrical and Computer Engineering

THIS PAGE INTENTIONALLY LEFT BLANK

ABSTRACT

The current United States Navy and Marine Corps warfighting concepts focus on distributed and decentralized operations to increase the lethality and security of the force as a whole. An amplified reliance on electrical energy to power weapon systems and the command and control structure, in conjunction with a dispersed force, escalates the logistical requirements for any unit. Renewable energy resources, such as solar radiation, may be a means of reducing this logistical burden; however, photovoltaic (PV) arrays must operate at their maximum power point for these systems to be more effective. This thesis studies the efficiencies of the controller for a PV power conditioning system implementing the two most common maximum power point tracking (MPPT) algorithms, "Perturb and Observe" and "Incremental Conductance." The system includes a commercial-off-the-shelf PV array, buck DC-DC converter, lead-acid batteries as its energy storage system and load, and an Opal-RT real-time simulator for rapid control prototyping. The efficiency of the MPPT controller was studied via simulation and improved through parameter optimization. The control algorithms were executed in a physical system using a hardware-in-the-loop testing configuration and the measured values were compared to the simulated results. Experimental testing confirmed the MPPT controller performed as designed and achieved the expected efficiency for the various solar irradiances and temperatures under which it was tested.

THIS PAGE INTENTIONALLY LEFT BLANK

TABLE OF CONTENTS

LIST OF FIGURES

THIS PAGE INTENTIONALLY LEFT BLANK

LIST OF TABLES

LIST OF ACRONYMS AND ABBREVIATIONS

A	amperes
A-D	analog-to-digital
D-A	digital-to-analog
DC	direct current
DOD	Department of Defense
EABO	Expeditionary Advanced Base Operations
ECU	electronic control unit
FPGA	field-programmable gate array
GREENS	Ground Renewable Expeditionary Energy Network System
GUI	graphical user interface
HIL	hardware-in-the-loop
IGBT	insulated gate bipolar transistor
INC	incremental conductance
I/O	input and output
MOSFET	metal-oxide semiconductor field-effect transistor
MPP	maximum power point
MPPT	maximum power point tracking
P&O	perturb and observe
PCU	power conditioning unit
PWM	pulse width modulation
PV	photovoltaic
RT	real-time
RT-LAB	Real-Time Laboratory
SIL	software-in-the-loop
SPACES	Solar Portable Alternative Communications Energy System
USMC	United States Marine Corps
V	volts
W	watts

THIS PAGE INTENTIONALLY LEFT BLANK

ACKNOWLEDGMENTS

I would like to thank my wife, Heather, for her love and support throughout our time in Monterey, especially during the COVID-19 shelter-in-place orders. I would also like to thank my son, Gabriel, and daughter, Addison, for the memories we've made in their short but eventful lives.

I would like to thank my family, especially my father, Samuel, and mother, Lynda, who have supported and loved me unconditionally over the years. Without them, I would not be where I am today.

Lastly, I would like to thank my advisor, Professor Giovanna Oriti, co-advisor, Professor Di Zhang, and Dr. Alexander Julian for their time and guidance throughout the entire research process.

THIS PAGE INTENTIONALLY LEFT BLANK

I. INTRODUCTION

A. MOTIVATION

The current warfighting concepts for the United States Navy and Marine Corps, Littoral Operations in a Contested Environment and Expeditionary Advanced Base Operations (EABO), focus on distributed and decentralized operations to increase the lethality and security of the force as a whole, specifically against peer adversaries [1]. The EABO concept, illustrated in Figure 1, "further distributes lethality by providing land-based options for increasing the number of sensors and shooters beyond the upper limit imposed by the quantity of seagoing platforms available. It espouses employing mobile, relatively low-cost capabilities in austere, temporary locations forward as integral elements of the fleet/ JFMCC" [2]. These distributed forces require electrical energy, primarily sourced from fossil fuels, to power weapons systems, command and control structures, and other materiel. Supply lines for fuel delivery from storage sites or ships may be vulnerable to attack, presenting a risk to mission and to those Marines and Sailors involved in fuel transport. Decreasing the demand for fuel to supply generators and tactical vehicles that currently power weapon systems and command and control structures results in longer sustained operations and reduced logistical requirements. Renewable energy resources, such as solar radiation, may be a means of reducing this logistical burden, increasing operational resilience, and decreasing costs.

Figure 1. Expeditionary Advanced Base Operations concept illustration. Source: [3].

Currently, the Marine Corps employs two power systems that use solar radiation as the primary energy source, Solar Portable Alternative Communications Energy System (SPACES) and Ground Renewable Expeditionary Energy Network System (GREENS). SPACES, shown in Figure 2, is a "lightweight, man-portable, renewable energy system designed to provide power for platoon and squad size unites operating in remote locations," specifically for recharging batteries used to power communications equipment [4]. The GREENS, depicted in Figure 3, is a larger, human-transportable power generation system capable of incorporating multiple energy sources, including photovoltaic (PV) arrays and generators, and storage components, including lithium ion and lead acid batteries, to provide sufficient power to fulfil the demand of a battalion combat operations center [4]. The overall efficiency of the renewable energy portion of these systems incorporating PV arrays is typically 96% for SPACES and ranges from 92% to 97% for GREENS [5], [6]. For these systems to be an even more effective, efficient, and reliable means of harvesting solar energy, the PV arrays must continuously operate at the maximum power point (MPP) given current environmental conditions, the configuration of controllers and PV arrays

should be optimized, and the power losses across electrical components must be reduced. Modern technology, including rapid control prototyping (RCP) simulators and more efficient energy storage and switching components, can be used to optimize control algorithms and decrease power losses across electrical components, potentially increasing the overall efficiency of the renewable energy portions of these systems.

Figure 2. SPACES. Source: [7].

Figure 3. GREENS. Source: [8].

B. RESEARCH OBJECTIVES

The primary research objective of this thesis is to study the efficiency of a maximum power point tracking (MPPT) controller for a PV power conditioning system connected to a direct current (DC) bus via a step-down switching DC-DC converter. In order to accomplish this primary objective, numerous secondary objectives are required.

The first objective is to create a simulation of the PV power system to optimize the parameters and study the efficiency of the controller implementing the two most common MPPT algorithms, "perturb and observe" (P&O) and "incremental conductance" (INC). Second, an experimental power system must be constructed using a commercial-off-the-shelf PV array, step-down switching DC-DC converter engineered from standard energy storage components and an insulated gate bipolar transistor (IGBT), lead-acid batteries as its energy storage system and load, and an Opal-RT real-time (RT) simulator for RCP and hardware-in-the-loop (HIL) implementation of the controller. The next objective is to modify and configure the simulation model for execution in the RT software and hardware input and output (I/O) interface. After modeling the system, the optimized control algorithms must be implemented in the experimental system using the RT simulator in a HIL testing configuration; and the voltage, current, and power produced by the PV array will be measured and compared to the simulated results. The last objective is to compare the power and efficiency of the optimized MPPT algorithms against one another to determine if one truly outperforms the other.

C. PREVIOUS WORK

There is a significant amount of literature discussing the numerous types of MPPT algorithms used in maximizing the energy from PV arrays, benefits and drawbacks of the different types of DC-DC converters used in solar energy harvesting, and PV array controller testing via RT software-in-the-loop (SIL) and HIL simulation. Esram and Chapman [9] published a summary article in which numerous PV array MPPT techniques, including P&O and INC, are thoroughly presented and the benefits and detriments of each are explained. The use of conventional DC-DC converter topologies, such as buck, boost, buck-boost and Cuk, for PV power conditioning are studied and compared in [10], [11],

[12]. In a previous thesis [13], Topping studied a PV system employing a boost DC-DC converter and interleaved boost converter that implemented the P&O and INC MPPT algorithms. Bailey [14] researched a PV system using a series-loaded resonant converter with galvanic isolation and compared two variants of the P&O algorithm, one solely requiring a voltage measurement and one requiring a voltage and current measurement. In [15], [16], [17], RT, SIL simulations were conducted on islanded and grid connected microgrids containing PV arrays controlled using the P&O and INC MPPT algorithms and a boost converter to demonstrate the load leveling capability of a battery on the DC bus, interaction of the PV system with the grid, and transient responses when shifting to from grid connected to islanding mode. Lastly, in [16], [18], the PV array, converter and/or inverter, and DC and AC bus were modeled in a RT simulator to test the performance of MPPT controller via HIL simulation and study the response of the controller to steady state, step, and ramp changes in solar irradiance, the lag produced in the pulse width modulation (PWM) signal from the controller, and DC bus voltage disturbances.

THIS PAGE INTENTIONALLY LEFT BLANK

II. BACKGROUND

This chapter reviews the implementation of DC-DC converters with digital controllers in the harvesting of solar energy, the two most common MPPT algorithms implemented in commercial systems today, and the use of HIL technology in PV array testing and applications.

A. STEP-DOWN DC-DC CONVERTER

For harvesting solar energy, DC- DC converters are used in conjunction with MPPT controllers to maximize the power extracted from the PV array via impedance matching and PV power regulation. This system, DC- DC converter controlled by a MPPT algorithm, is known as a smart converter or power conditioning unit (PCU) [10]. The impedance matching stage of the PCU can include different structures of the DC-DC converters which "vary according to arrangement complication, selling cost, effectiveness, number of passive electronic components, current ripple at their entry and exit, tracking and non-tracking regions, static gain polarity and value, and resistance adaptation rate" [19]. Three types of DC-DC converters, step-up, step-down, and step-up or down, can be utilized for impedance matching and voltage control applications depending on the rated voltage of the PV source and the DC bus voltage. In this thesis, the step-down, or buck, converter is used since the DC bus voltage is lower than the voltage output of the PV array.

A typical buck converter, shown in Figure 4, is a switching converter that produces an average output voltage lower than the input voltage. Such topology is appropriate to charge batteries rated at a lower voltage than the PV source from which they are charged. The output voltage of the buck converter, V_o, is controlled by varying the duty ratio, D, of the switch; defined by the ratio of time the switch is spent on, t_{on}, to the overall switching period, T_s. The switching voltage is illustrated in Figure 5, where the duty ratio is also shown. Referencing Figure 4, when the switch is closed, the diode becomes reverse biased and the input voltage and current provide energy to the load as well as the inductor; and when the switch is open, the current from the inductor flows through the diode, transferring some of its stored energy to the load [20]. Assuming ideal electrical components, no

voltage losses across the switch, diode, or inductor, as the switch turns on and off, the voltage across the diode, v_{oi}, resembles that of a square wave. Therefore, the amplitude of the square wave is equivalent to the input voltage, V_d, when the switch is closed, while it is zero when the switch is open. The use of a low-pass filter, consisting of an inductor, L, and a capacitor, C, diminishes the output voltage fluctuations across the diode, and results in a constant DC output component, V_o, and the harmonics at the switching frequency, $f_{sw,}$ and its multiples, as shown in Figure 5. In order to reduce the switching frequency ripple caused by the harmonics at the switching frequency and beyond, the corner frequency, f_c, of the low-pass filter, a function is selected to be much lower than the switching frequency, as illustrated in Figure 6 [20]. Also noted from Figure 4, the average output current of a buck converter, I_o, is equal to that of the inductor current, i_L, since the average capacitor current during steady state operation is zero.

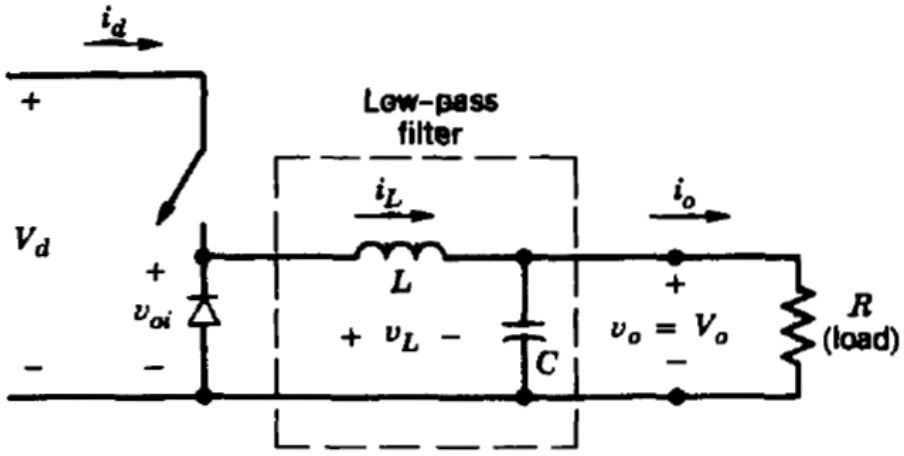

Figure 4. Buck (step-down) DC-DC converter. Source: [20].

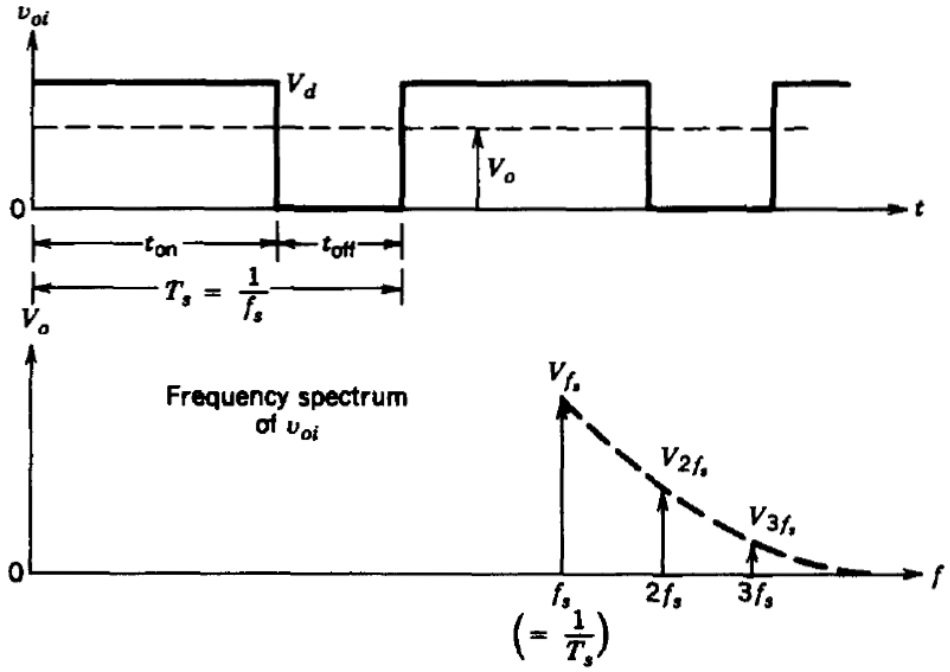

Figure 5. Buck (step-down) diode voltage waveform with frequency spectrum. Source: [20].

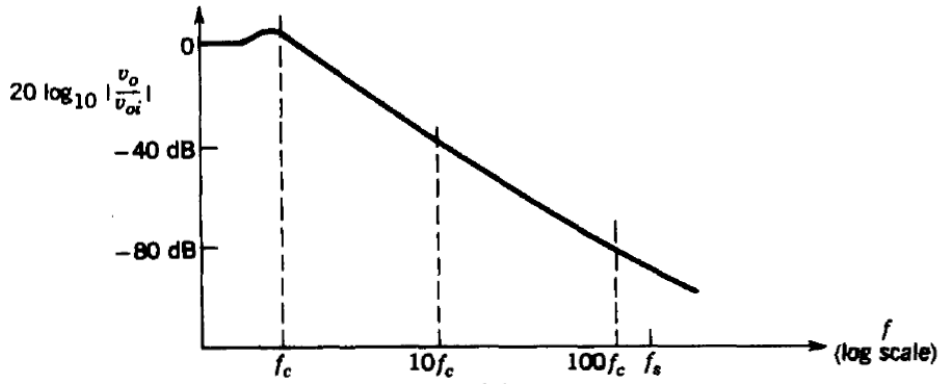

Figure 6. Buck (step-down) low-pass filter frequency spectrum. Source: [20].

B. MAXIMUM POWER POINT TRACKING

In order to harvest the largest amount of solar energy from the PV array(s), the MPP of the array(s) must be tracked. MPPT algorithms are designed to find the voltage, V_{MPP}, and current, I_{MPP}, at which the PV array must operate to obtain the maximum power output, P_{MPP}, for a given irradiance and temperature.

Two characteristic curves are used when creating MPPT algorithms and studying energy harvesting from PV arrays given a specified temperature and irradiance: (1) power versus voltage, as shown in Figure 7 and Figure 9, and (2) voltage versus current, as displayed in Figure 8 and Figure 10. Figure 7 and Figure 8 depict the effect of irradiance on the characteristic curves at a temperature of 25°C, the standard temperature for which solar panels are rated and tested, while Figure 9 and Figure 10 show the effect of temperature given an irradiance of 1000 W/m^2, the standard irradiance for which solar panels are rated and tested. To note, these characteristic curves were created using the plot function within the PV array Simscape block in Simulink using the parameters for a Solartech SPM090P 90 W PV array.

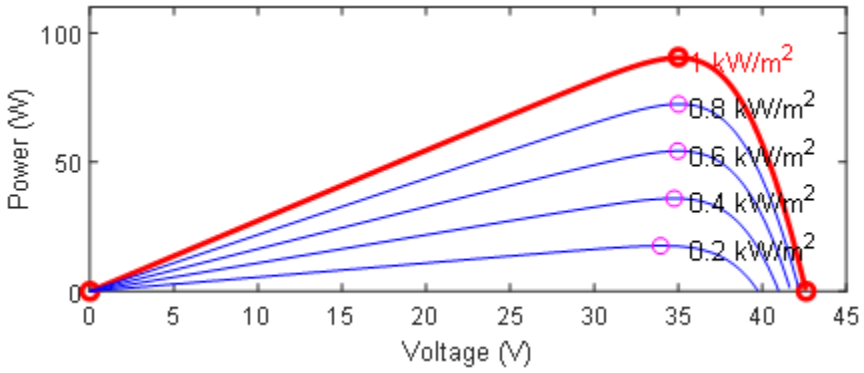

Figure 7. Solartech SPM090P PV array P-V characteristic curves at 25°C

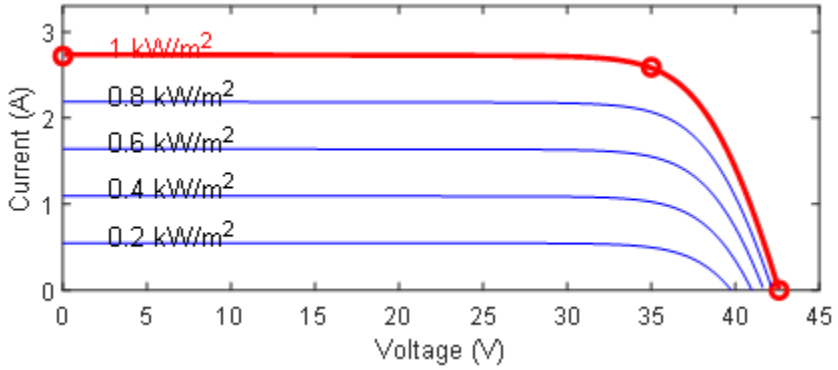

Figure 8. Solartech SPM090P PV array I-V characteristic curves at 25°C

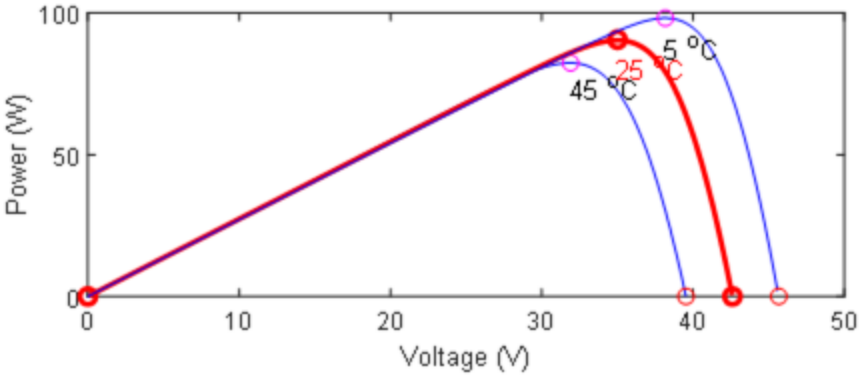

Figure 9. Solartech SPM090P PV array P-V characteristic curves at 1000 W/ m^2

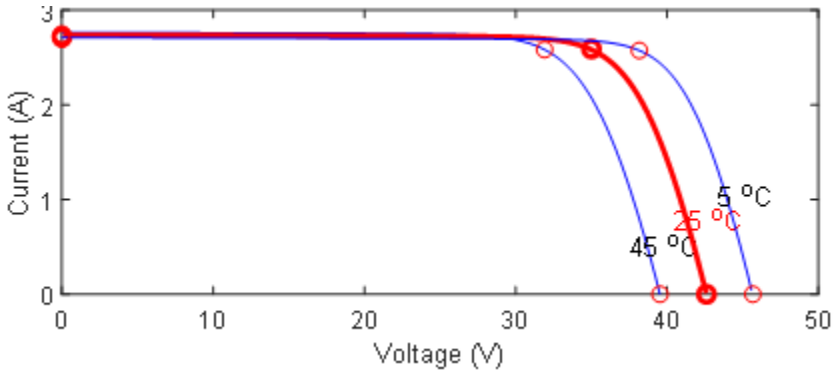

Figure 10. Solartech SPM090P PV array I-V characteristic curves at 1000 W/ m^2

On each of the plots in Figures 7 through 10, the MPP, open-circuit voltage, V_{OC}, and short-circuit current, I_{SC}, are marked with circles. The V_{OC} is the highest possible voltage the PV array can produce and is determined when the current is zero, and therefore is not feasible when considering PV array voltage capabilities in practical applications. Similarly, I_{SC} is the highest possible current the PV array can produce and is determined when the voltage is zero. Three key observations in regard to the power, current, and voltage characteristics of a PV array can be made from analyzing Figure 7 through Figure 10:

- As depicted in Figure 7 and Figure 9, each non-linear power curve contains one MPP per specified irradiance. For each V_{MPP}, there is a

corresponding $I_{MPP,}$ noted on the characteristic I-V curve in Figure 8 and Figure 10. To note, when partially shaded conditions exist, i.e., there is less irradiance on one module of an array than the others, multiple local maxima may be present, but only one real MPP exist [9].

- As illustrated in Figure 7 and Figure 8, as the solar irradiance varies, the power at the MPP for the PV array varies proportionally. A variance in solar irradiance causes minimal alteration to both the V_{MPP} and V_{OC}, but a proportional change to the I_{MPP} and I_{SC}.

- Referencing Figure 9 and Figure 10, as the temperature of the panel increases, the maximum power output decreases and vice versa. An increase in temperature causes both the V_{MPP} and V_{OC} to decrease while having minimal effect on the I_{MPP} and I_{SC}.

1. MPPT Algorithms

Currently, there are numerous methods for tracking the MPP of a PV array using a DC-DC converter; this thesis will focus on the implementation of two of the most commonly used algorithms, P&O and INC. Each algorithm determines the power produced by the solar panel with respect to its voltage and then modifies the control parameters in order to locate the MPP of the system.

a. Perturb and Observe

P&O algorithms are commonly used in MPPT applications due to their simple structure and control logic [21]. Referencing Figure 7, as the voltage of the PV array increases, the power increases when operating left of the MPP but decreases when operating to the right. On the other hand, as the voltage of the PV array decreases, the power decreases when operating left of the MPP but increases when operating to the right. Therefore, if the power produced by the PV array increases, the subsequent perturbation, whether incrementing or decrementing the voltage, remains unchanged; but when the power produced by the PV array decreases, the ensuing perturbation reverses direction [9]. A summary of this algorithm is noted in Table 1.

Table 1. Summary of P&O algorithm. Source: [21].

Perturbation	Change in Power	Next Perturbation
Positive	Positive	Positive
Positive	Negative	Negative
Negative	Positive	Negative
Negative	Negative	Positive

There are two complications with the P&O algorithm: operating at the MPP once reached and MPPT under rapidly changing irradiance conditions. As the system reaches the MPP of the PV array, it tends to oscillate about that power vice staying constant due to the size of the perturbation. The primary means of minimizing or eliminating this power oscillation is reducing the size of the perturbation step used in the algorithm [9]. Reducing the perturbation step size, however, causes issues for MPPT under rapidly changing environmental conditions, as illustrated in Figure 11.

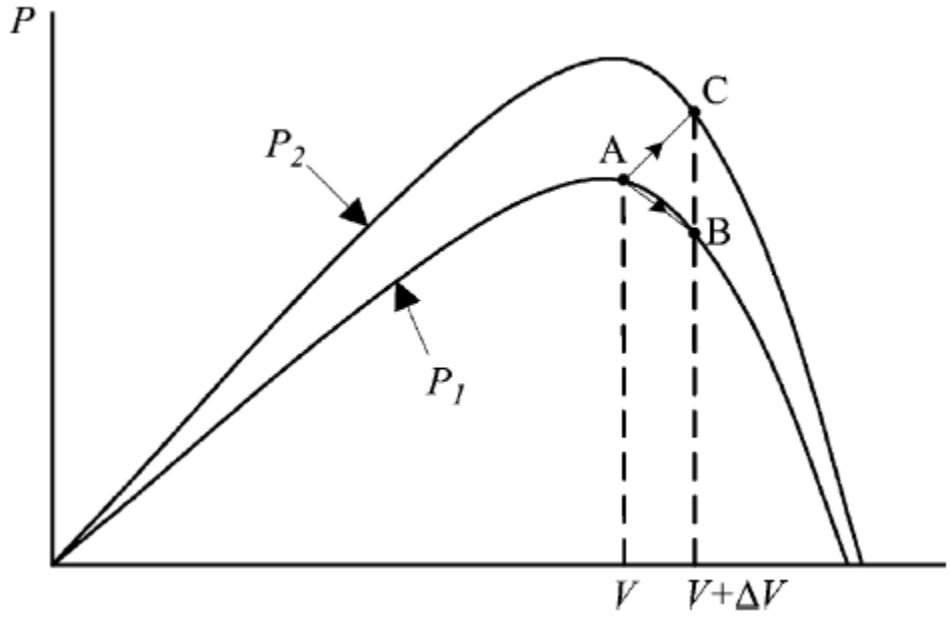

Figure 11. Divergence of P&O for MPP. Source: [9].

Starting from an operation point A, if atmospheric conditions stay approximately constant, a perturbation, ΔV, in the PV voltage, V, will bring the operating point to B and the perturbation will be reversed due to a

> decrease in power. However, if the irradiance increases and shifts the power curve from P_1 to P_2 within the sampling period, the operating point will move from A to C. This represents an increase in power and the perturbation is kept the same. Consequently, the operating point diverges from the MPP and will keep diverging if the irradiance steadily increases. [9]

Therefore, a smaller step means the algorithm will not be able to track changes in power as fast as a larger step, causing the algorithm to lock on to the wrong MPP for the solar array. A larger step, on the other hand, will cause the algorithm to oscillate more about the MPP, reducing the effectiveness of the controller.

The P&O flowchart shown in Figure 12 illustrates the measurements, calculations, and logic of the algorithm. First, the voltage, *V[k]*, and current, *I[k]*, produced by the PV array are measured, and an equivalent power, *P[k]*, is calculated and compared to the previous power, *P[k-1]*, stored in the controller. If the two values are equivalent, the duty cycle or reference voltage remains the same; but if the powers are different, the controller determines if the power increased or decreased. After determining the change in power, ΔP, the controller then looks to determine if the voltage increased or decreased, leading to four possible duty cycles or reference voltage perturbations. The four possible combinations for the duty cycle control technique are: (1) if the power and voltage increase, the duty cycle decreases by the duty cycle step, Δd, (2) if the power increases but the voltage decreases, the duty cycle increases by Δd, (3) if the power and voltage decrease, the duty cycle decreases by Δd, and (4) if the power decreases but the voltage increases, the duty cycle increases by Δd. The reference voltage control technique follows the same steps as the duty cycle control technique, however, the sign of the reference voltage perturbation, ΔV_{ref}, is always the opposite of the duty cycle perturbation previously discussed.

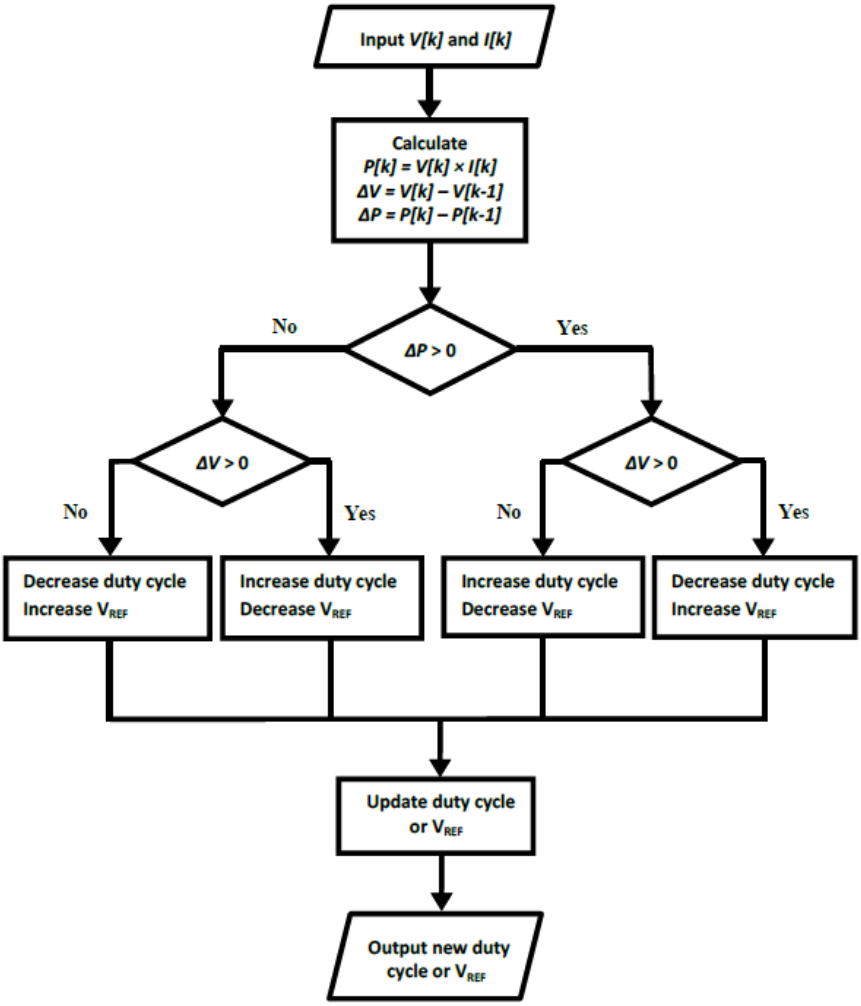

Figure 12. Perturb and Observe flowchart. Source: [13].

b. Incremental Conductance

The INC algorithm is designed around the slope of the PV array power curve, found in Figure 7, being positive left of the MPP, zero at the MPP, and negative right of the MPP [9]. The slope of the power curve can also be depicted by the derivative of the power with respect to voltage, *dP/dV*, as listed in Table 2.

Table 2. Continuous PV array power curve slope comparisons with respect to the MPP. Source: [9]

$dP/dV = 0$	MPP
$dP/dV > 0$	left of MPP
$dP/dV < 0$	right of MPP

Understanding that power, *P*, is equivalent to the product of the voltage, *V*, and the current, *I*, this continuous-time derivative can be simplified into two variables, voltage and current.

$$\frac{dP}{dV} = \frac{d(VI)}{dV} = I + V\frac{dI}{dV}$$

Discretizing the equation, setting it equal to zero, the slope at the MPP of the PV array, and solving for the change in current, ΔI, over the change in voltage, ΔV, enables Table 2 to be written in terms of voltages and currents, as shown in Table 3.

Table 3. Discrete PV array power curve slope comparisons with respect to the MPP. Source: [9]

$\Delta I/\Delta V = -I/V$	MPP
$\Delta I/\Delta V > -I/V$	left of MPP
$\Delta I/\Delta V < -I/V$	right of MPP

The INC MPPT algorithm is executed by comparing the instantaneous conductance (I/V) to the incremental conductance ($\Delta I/\Delta V$). Once the MPP is reached, the PV array operates at that point unless a change in current, ΔI, is noted, indicating a change in the irradiance or temperature of the PV array [9]. As with the P&O algorithm, the incremental step sized determines how fast the INC algorithm can track changes in power as well as the degree of oscillation around the MPP.

The INC flowchart, depicted in Figure 13, illustrates the measurements, calculations, and logic of the algorithm. First, the voltage, *V[k]*, and current, *I[k]*, produced by the PV array are measured and compared to their previous values, *V[k-1]* and *I[k-1]*, respectively. The change in current, ΔI, is then divided by the change in voltage, ΔV, to

produce the incremental conductance. The change in voltage is also used in the next step of the algorithm. If there is no change in voltage, $\Delta V = 0$, then only the change in current, ΔI, is used for the remainder the algorithm; however, if there is a voltage change, the incremental conductance, $\Delta I/\Delta V$, is compared to the instantaneous conductance, I/V. If there is no change in voltage, the three possible combinations for the duty cycle control technique are: (1) if there is no change in current, $\Delta I = 0$, then there is no perturbation to the duty cycle, (2) if there is a change in current greater than zero, $\Delta I > 0$, the duty cycle decreases by the duty cycle step, Δd, and (3) if there is a change in current less than zero, $\Delta I < 0$, the duty cycle is increased by Δd. If there is a change in voltage, there are three possible combinations for the duty cycle control technique. First, if the sum of the incremental conductance and the instantaneous conductance is zero, $\Delta I/\Delta V + I/V = 0$, then there is no perturbation to the duty cycle. Second, if the sum of the incremental conductance and instantaneous conductance is greater than zero, $\Delta I/\Delta V + I/V > 0$, the duty cycle decreases by Δd. Third, if the sum of the incremental conductance and instantaneous conductance is less than zero, $\Delta I/\Delta V + I/V < 0$, the duty cycle increases by Δd. As with the P&O algorithm, the reference voltage control technique follows the same steps as the duty cycle control technique, however, the sign of the reference voltage perturbation, ΔV_{ref}, is always the opposite of the duty cycle perturbation previously discussed.

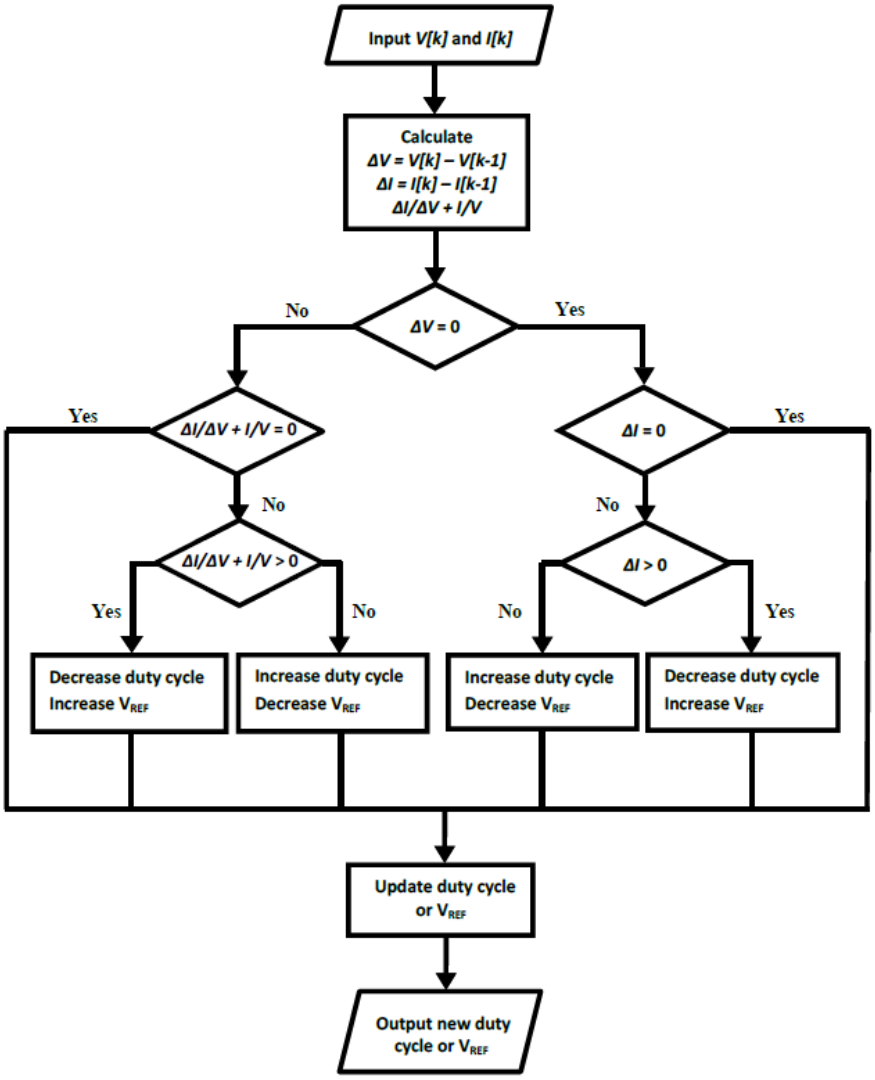

Figure 13. Incremental conductance flowchart. Source: [13].

2. Control Techniques

Two common control techniques used to drive the PWM of the DC-DC power converter include the duty cycle and reference voltage methods.

a. Duty Cycle

Once the chosen MPPT algorithm is executed as previously described, the duty cycle perturbation, Δd, is added to the previous duty cycle to produce a new duty cycle. This new duty cycle is then converted into the pulse width modulated signal used to control

the switch of the DC- DC converter appropriately, enabling the PV array to operate near the MPP. This process is noted in Figure 14.

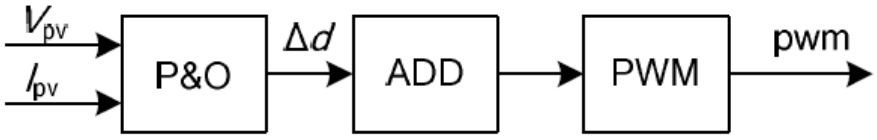

Figure 14. Control schematic of duty cycle P&O for MPPT. Source: [22].

This duty cycle control technique is easier to implement when compared to the reference voltage technique, however some downfalls do exist. Although it is capable of efficiently tracking the MPP at lower power ranges, it is not ideal with larger fluctuations in power since it is restricted by the minimum duty cycle perturbation, Δd, in practice [22].

b. Reference Voltage

The reference voltage technique, depicted in Figure 15, is slightly more complicated, requiring more components and computations, than the duty cycle method. Once the change in reference voltage, ΔV_{ref}, is determined by the MPPT algorithm, it is added to the previous value for the reference voltage, V_{ref}. After, the current PV array voltage, V_{PV}, is subtracted from the new reference voltage. This voltage difference is then sent through a proportional and integral (PI) controller and converted to a PWM signal to control the switch of the DC-DC converter.

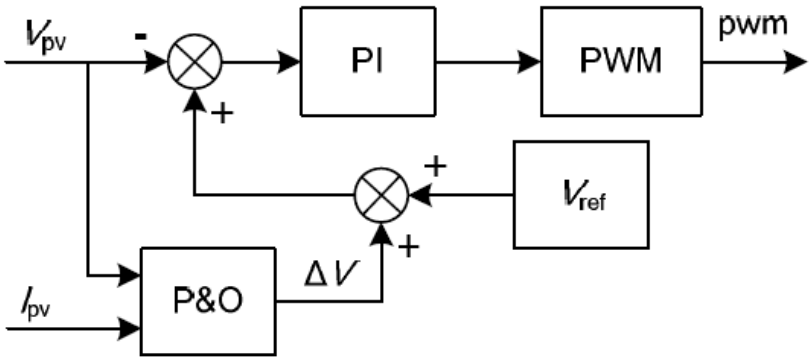

Figure 15. Control schematic of reference voltage P&O for MPPT. Source: [22].

This reference voltage control technique is more complex to implement when compared to the duty cycle method as it requires additional tuning of a PI controller in the computation. However, the fluctuation in output power using the reference voltage technique is reduced compared to that of the duty cycle method, even with the same perturbation quantity for ΔV_{ref} and Δd [22].

III. MODELING AND SIMULATION

This chapter discusses the stand-alone PV power system architecture and physics-based model developed for analysis. Simulations of the different MPPT methods are presented using MATLAB and Simulink to identify the control parameters that yield maximum efficiency.

A. STAND-ALONE PV SYSTEM ARCHITECTURE

The stand-alone power system analyzed in this thesis is depicted in Figure 16. As noted in the figure, the system consists of a single PV array, buck DC-DC converter controlled by a duty cycle driven PWM signal, a DC load, and MPPT controller requiring both voltage and current measurements from the PV array. This architecture was assembled in hardware with a 24 V battery pack used as the load.

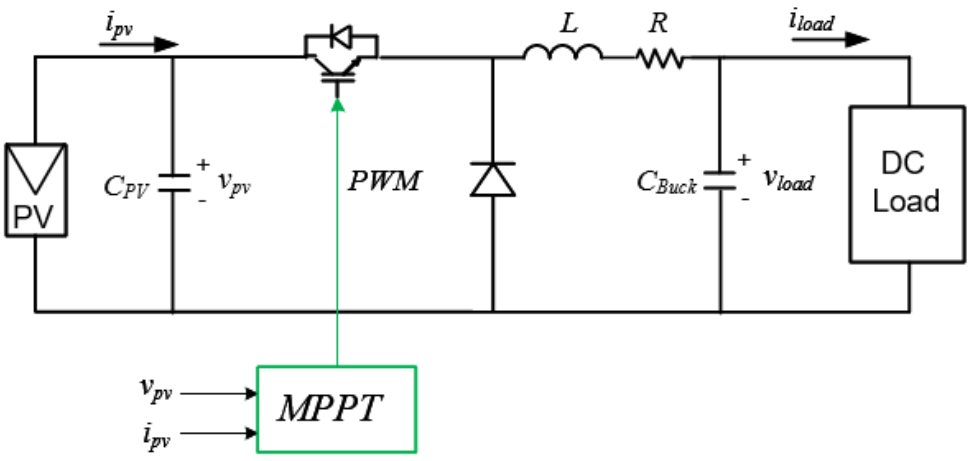

Figure 16. PV power system with DC bus

B. PHYSICS-BASED MODEL

A physics-based model of the laboratory PV system was developed and implemented in Simulink with the same component parameters used in the hardware. The block diagram shown in Figure 17 was extracted from the Simulink software implementation and each block is presented in detail in the following sections.

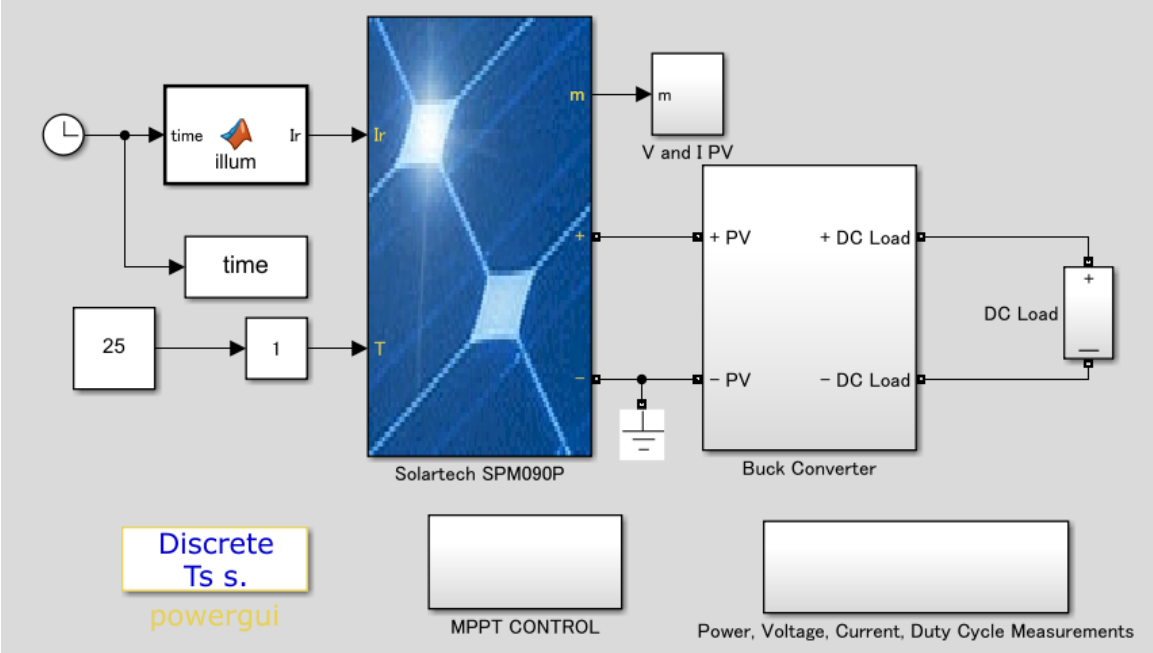

Figure 17. Simulink model of PV power system with DC bus

1. PV Array

The PV array was modeled using the Simscape PV Array model and parameters of a Solartech SPM090P PV array. Simscape is a toolbox within the Simulink environment which provides models and physical connections that directly integrate with other Simulink components [23]. Although the Simscape PV array model offers a variety of preset PV array models currently on the market, the one being simulated, Solartech SPM090P, was not available. The parameters of the PV array, listed in Table 4, were inserted into a generic PV array block to replicate the power, temperature, and irradiance characteristics of the panel.

Table 4. Solartech SPM090P PV array characteristics. Source: [24]

maximum power (P_{max})	90.65 W
cells per module (Ncell)	36
open circuit voltage (Voc)	42.6 V
short-circuit current (Isc)	2.72 A
voltage at MPP (Vmp)	35 V
current at MPP (Imp)	2.59 A
temperature coefficient of Voc	-0.36 %/C
temperature coefficient of Isc	0.05 %/C

The MPP characteristics of the Solartech SPM090P PV array at an operating temperature of 25°C and irradiances varying from 1000 W/m^2 to 200 W/m^2 are illustrated in Figure 7 and Figure 8 and listed in Table 5.

Table 5. Solartech SMP090P MPP characteristics at 25°C

Irradiance (W/m^2)	**Voltage (V)**	**Current (A)**	**Power (W)**
1000	35	2.59	90.65
800	35	2.07	72.47
600	34.97	1.55	54.30
400	34.76	1.03	35.95
200	33.95	0.52	17.59

Input requirements for the PV array model include the irradiance from the sun in W/m^2 and the temperature of the solar cells in degrees Celsius. A user defined MATLAB function in conjunction with the simulation clock controlled the irradiance input for the PV array block to automate different irradiances throughout the simulation. This enabled the system to step through numerous, specific irradiances without having to adjust using a slider gain or restart the simulation for each desired irradiance. The irradiance stepped down 200 W/m^2 each second, from 1,000 W/m^2 to 200 W/m^2, for the duration of the simulation. A constant block with a slider gain was used to control the temperature of the PV array since this parameter doesn't change as rapidly as solar irradiance.

Outputs of the PV array model include measurements for the PV array voltage, V_{PV}, PV array current, I_{PV}, and current through the diode within the model (not to be used during

this thesis). To minimize the effects of noise on these measurements, the signals passed through a software based, first-order, low pass filter with a cutoff frequency of 5 kHz prior to their use in the MPPT controller and data analysis.

2. MPPT Controller

The MPPT controller, shown in Figure 18, can implement either a modified P&O or basic INC MPPT algorithm within the user defined MATLAB function and a PWM generator. Inputs to the function include duty cycle parameters and sampled measurements of the filtered PV array voltage, $V_{PV,}$ and current, I_{PV}. The duty cycle parameters include the initial duty cycle, duty cycle perturbation quantity, Δd, and the maximum and minimum allowable duty cycle the function can output. The function uses these parameters in conjunction the desired MPPT algorithm to compute the appropriate duty cycle for the PV array to operate at the MPP. This duty cycle passed through a PWM generator with a preset carrier or switching frequency to control the switch of the DC-DC converter.

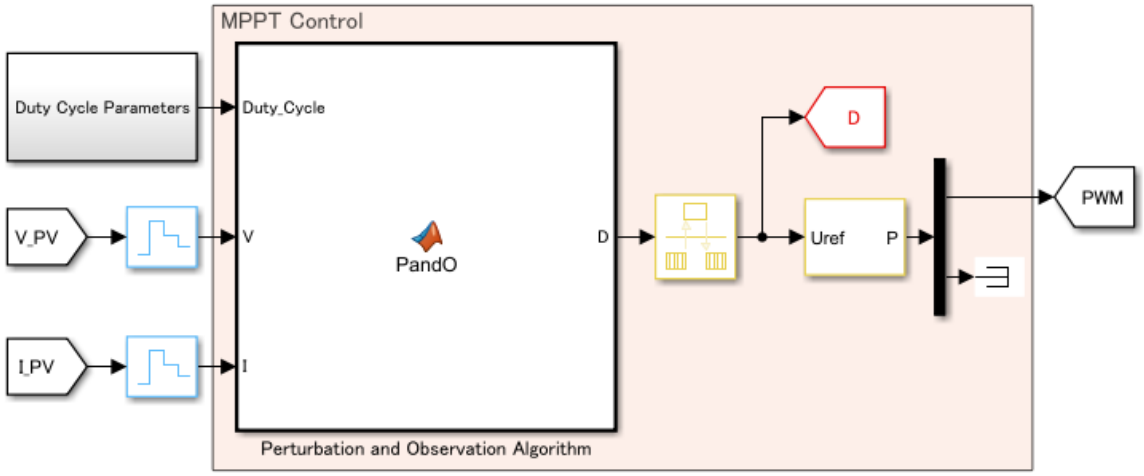

Figure 18. Simulink model of MPPT controller

The P&O algorithm used in the simulation mimics that of the conventional P&O algorithm defined in the theory chapter, only containing one small adjustment to improve performance during steady state operations. With the conventional algorithm, the duty cycle remains the same between control steps only when there is zero change in power,

ΔP. Comparing the change in power to zero vice a small numerical value ensures the algorithm will perturb the previous duty cycle for any miniscule change in power, adjusting the duty of the system vice keeping it the same as the previous value. In the P&O algorithm used in this thesis, the absolute value of the change in power, $|\Delta P|$, is first compared to an arbitrary small number, 0.001 W. If the magnitude of change in power is less than or equal to 0.001 W, the previous duty cycle is used for the output of the algorithm. If the magnitude of the change in power is greater than 0.001 W, the P&O algorithm follows the logic of the conventional algorithm for control steps when the change in power did not equal zero. This minor adjustment improved the operation of the controller under steady state solar irradiance condition in simulation, but it did not improve steady state operation in experimental testing.

3. Buck DC-DC Converter

The buck, or step-down, DC-DC converter was modeled as shown in Figure 19, using components from the Simscape electrical library including a Semikron IGBT, inductors, and capacitors. The parameters used in the model are listed in Table 6 and match the physical components to be tested. A capacitor was placed before the switch of the converter to ensure a stable voltage signal, V_{PV}, passed into the converter from the PV array. The PWM signal from the MPPT controller drove the switch, Semikron IGBT modeled with a forward voltage drop of 2 V to simulate the physical system, to ensure the converter operated in a means that enabled the MPP of the PV array to be tracked while maintaining a constant voltage on the DC bus.

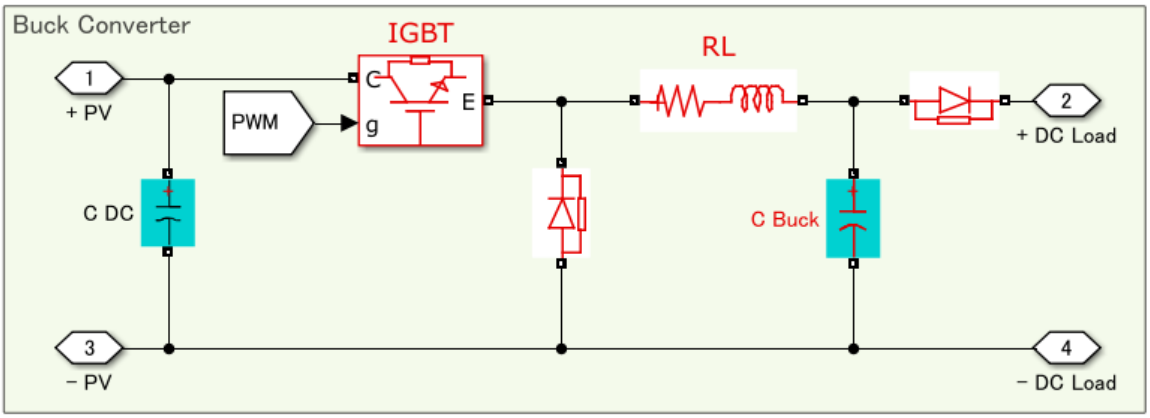

Figure 19. Simulink model of a buck converter

Table 6. Buck converter parameters

C_{DC}	1100 µF
R	0.1 Ω
L	232 µH
C_{Buck}	1000 µF

4. Other Components

a. Load

A widely known use of PV arrays is to charge energy storage devices since they are not reliable sources of DC energy throughout an entire day; therefore, the DC load chosen for this thesis included of a 24 V battery. Using a battery for the load also ensured the DC bus maintained a constant voltage and the load drew the maximum available current from the PV array. The battery was modeled as a DC voltage source for the simulation portion of the thesis.

b. Powergui Block

The “powergui” block, a required environmental block for Simscape electrical specialized power system models, was implemented in the top-level of the diagram. From this block, the type of simulation was set to discrete and the sample time was set to that of the fixed time step of the overall simulation.

C. SIMULATION RESULTS

The stand-alone PV power system described in the previous section was simulated using both the P&O and INC MPPT algorithms while varying the parameters for the converter switching frequency, f_{sw}, duty cycle perturbation quantity, Δd, and MPPT sampling frequency, $f_{MPPT,}$ to determine their effect on the ability of the controller to track the MPP. The simulation was executed using a fixed time step of 10 μs, PV array temperature measuring 25°C, and irradiance stepped down as previously described.

The objective was to determine which parameters and algorithm enabled the controller to track the MPP of the PV array to the greatest extent possible throughout the duration of the simulation. Thus, the tracking performance of the MPPT algorithm and controller were evaluated by means of the MPPT efficiency:

$$\eta_{MPPT} = \frac{P_{PV}}{P_{MPP}},$$

where P_{PV} is the power extracted from the PV array and P_{MPP} is the maximum power available from the PV array per specified solar irradiance. The efficiencies at each irradiance quantity for the specified parameters and algorithm are noted in the following sections.

1. Switching Frequency

The effect of the DC-DC converter switching frequency on the MPPT efficiency of the controller was determined by simulating the PV power system using the P&O algorithm, a fixed duty cycle perturbation of 0.001, MPPT sampling frequency of 100 Hz, and converter switching frequencies of 1, 5, and 10 kHz. As noted in Figure 20 and Table 7, the faster switching frequencies of 5 and 10 kHz significantly outperformed the 1 kHz frequency. The 5 kHz frequency proved more efficient at the higher irradiances of 1,000, 800, and 600 W/m^2, while the 10 kHz frequency tracked the MPP more efficiently at the lower irradiances.

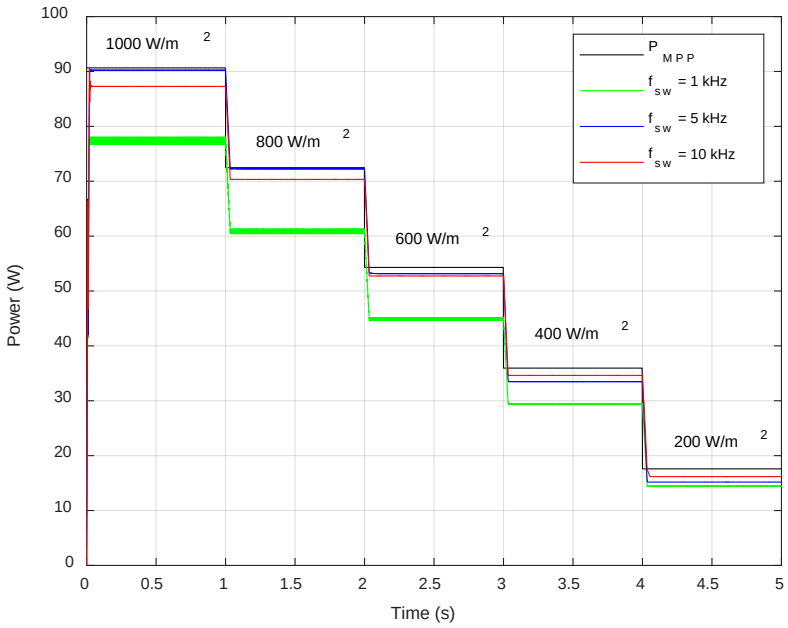

Figure 20. Simulated PV array power comparing converter switching frequencies

Table 7. Simulated MPPT efficiencies for varied converter switching frequencies

Irradiance (W/m^2)	**MPPT Efficiency (%)**		
	f_{sw} = 1 kHz	**f_{sw} = 5 kHz**	**f_{sw} = 10 kHz**
1000	85.40	99.53	96.29
800	84.02	99.70	97.06
600	82.66	97.88	97.12
400	81.78	93.10	96.31
200	82.04	86.33	91.97

The settling times, how fast the controller reached and maintained 2% of its steady-state value from when the simulation initiated, for each converter switching frequency were also analyzed to determine which switching frequency enabled the controller to track the MPP faster. As noted in Figure 21, the 1 and 10 kHz switching frequencies enabled the system to achieve a 0.0187 second and 0.0233 second settling times, respectively, although the power produced by the systems only reached 85.40% and 96.29% of its theoretical

maximum power. The 5 kHz switching frequency, on the other hand, produced a 0.0214 second settling time at 98% of the systems theoretical maximum power.

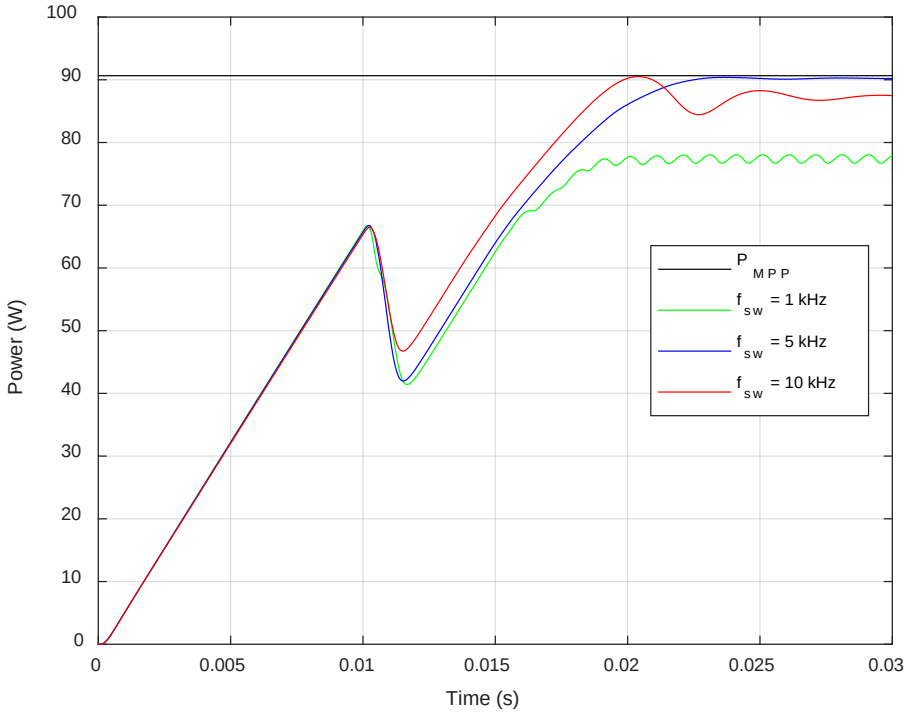

Figure 21. Initial transient of simulated PV array power comparing converter switching frequencies

Therefore, the 5 and 10 kHz switching frequencies proved much more efficient and effective in tracking the MPP of the PV array when compared to the lower switching frequency of 1 kHz. Although the 1 kHz switching frequency produced a faster settling time, the steady-state power achieved was a mere 85.40% of the theoretical maximum power per given irradiance, an unacceptable efficiency.

2. Duty Cycle Perturbation Quantity

The effect of the duty cycle perturbation quantity, Δd, on the MPPT efficiency of the controller was determined by simulating the PV power system using the P&O algorithm, MPPT sampling frequency of 100 Hz, 5 kHz and 10 kHz switching frequencies,

and fixed and varying duty cycle perturbation quantities of 0.001, 0.005, and 0.01. To note, the 1 kHz switching frequency was dropped for comparison purposes due to its poor performance in the previous section.

The algorithm used for varying the perturbation quantity in the MPPT control algorithm depended on changes in the power measured from the PV array. In order to use each of the fixed perturbation quantities in the algorithm, three distinct cases were created to account for changes in power: (1) if the magnitude of the change in power, $|\Delta P|$, is less than 1% of the previous power measurement, the duty cycle perturbation quantity, Δd, equaled 0.005, (2) if $|\Delta P|$ is greater than or equal to 1% but less than 5% of the previous power measurement, the duty cycle perturbation quantity equaled 0.01, and (3) if $|\Delta P|$ is greater than or equal to 5% of the previous power measurement, the duty cycle perturbation quantity equaled 0.02. This algorithm, in conjunction with the conventional P&O MPPT algorithm, should enable the PV array to track the MPP more efficiently. It provides smaller changes in duty cycle with smaller changes in irradiance and power, and larger changes in duty cycle with larger changes in irradiance and power.

The simulation results for the PV power system with a 5 kHz switching frequency are depicted in Figure 22 and Table 8. It can be noted that the smallest duty cycle perturbation quantity of 0.001 enabled the controller to track the MPPT more efficiently at the 800 W/m^2 irradiance level. The varying duty cycle perturbation quantity, however, proved more efficient throughout the range of simulated irradiances, especially at 400 W/ m^2 irradiance level. At the lowest irradiance, 200 W/m^2, the largest fixed duty cycle perturbation quantity of 0.01 proved slightly more efficient than the varying duty cycle perturbation quantity. Although not depicted, it is also important to note that the initial settling times for each perturbation quantity were identical, equaling that of the 5 kHz converter switching frequency noted in the previous section, 0.0214 seconds. Therefore, for the PV power system implementing the 5 kHz switching frequency and MPPT controller sampling at 100 Hz, a varying duty cycle perturbation quantity enabled the controller to more efficiently track the MPPT of the PV array for the span of irradiances simulated.

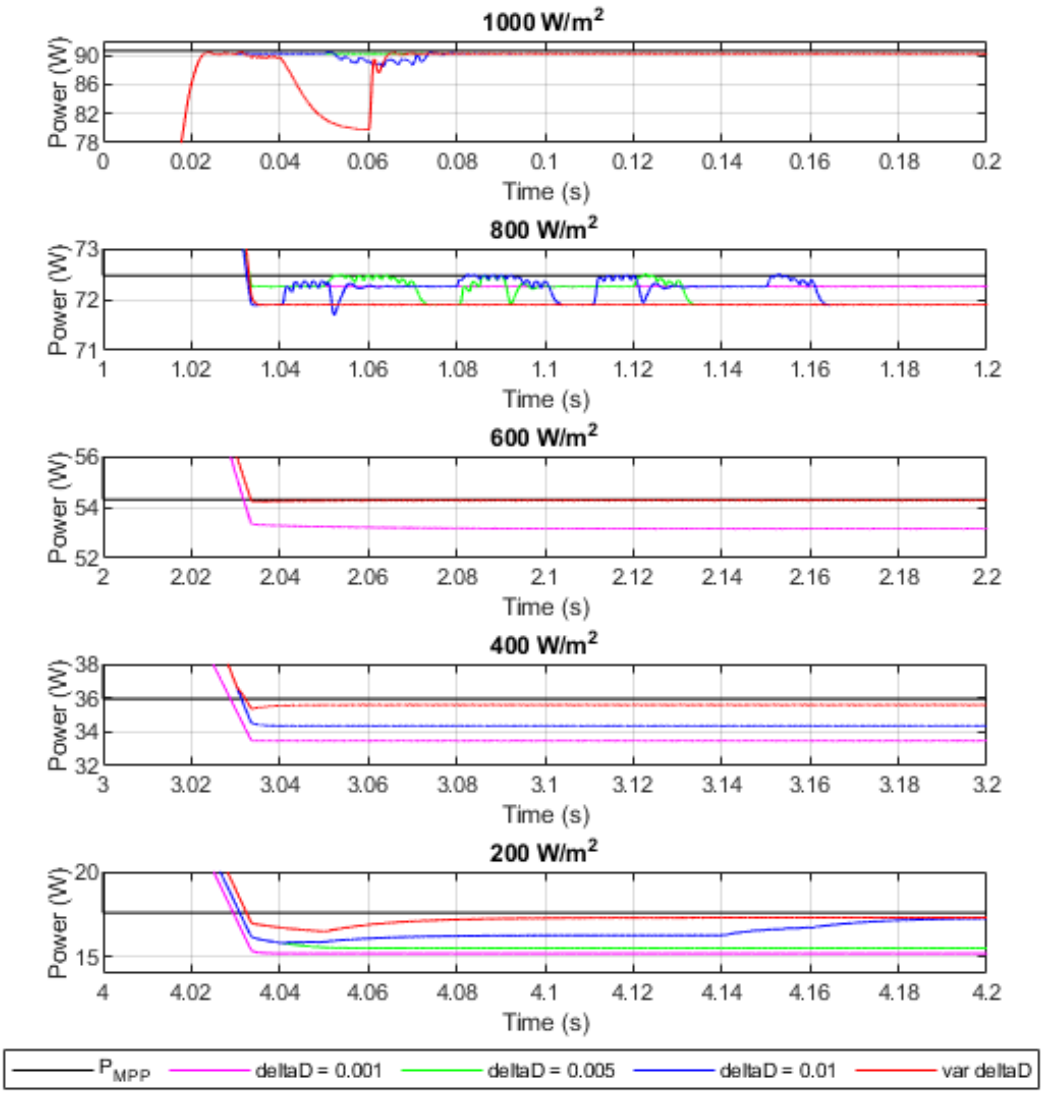

Figure 22. Simulated PV array power using 5 kHz switching frequency comparing duty cycle perturbation quantities

Table 8. Simulated MPPT efficiencies using 5 kHz switching frequency for various duty cycle perturbation quantities

Irradiance (W/m^2)	**MPPT Efficiency (%)**			
	Δd = 0.001	**Δd = 0.005**	**Δd = 0.01**	**Varying Δd**
1000	99.53	99.53	99.53	99.53
800	99.70	99.21	99.21	99.21
600	97.88	99.94	99.94	99.94
400	93.10	95.55	95.55	99.01
200	86.33	88.11	98.99	98.33

The simulation results for the PV power system implementing a 10 kHz converter switching frequency are depicted in Figure 23 and Table 9. As shown in the results, the controller efficiencies for each duty cycle perturbation quantity were identical for the 1,000, 800, 600, and 400 W/m^2 irradiances. Contrary to the system with the 5 kHz switching frequency, the controller implementing the varying duty cycle perturbation quantity proved more efficient at the 200 W/m^2 irradiance when compared to the fixed perturbation quantities. Also, it is also important to note that the initial settling times for each perturbation quantity were again identical, equaling that of the 10 kHz switching frequency noted in the previous section, 0.0233 seconds. Therefore, for the PV power system implementing the 10 kHz switching frequency and MPPT controller sampling at 100 Hz, the duty cycle perturbation quantity created little impact on the efficiency of the MPPT controller for the span of simulated irradiances, only improving the performance of the controller at the lowest irradiance.

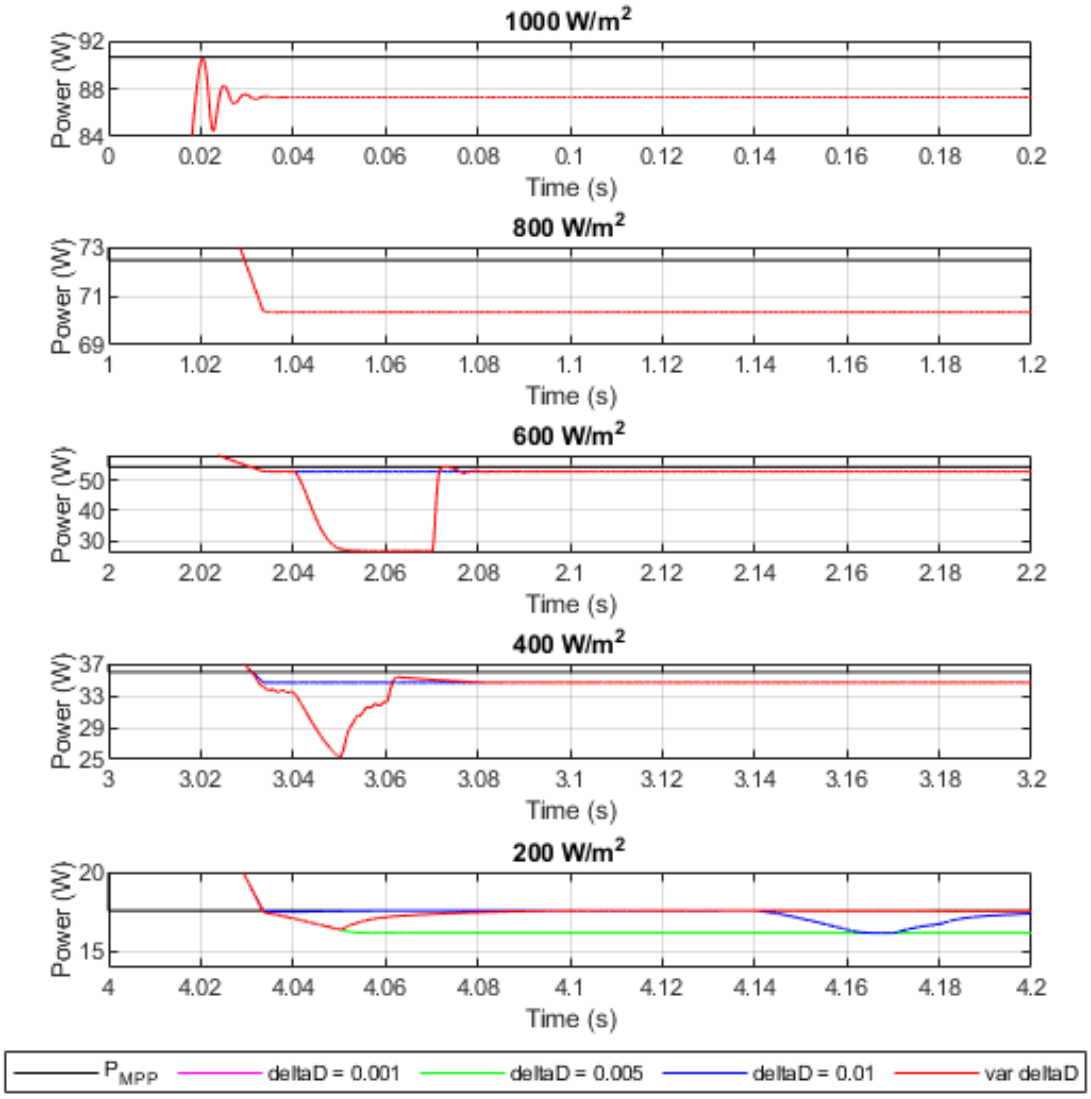

Figure 23. Simulated PV array power using 10 kHz switching frequency comparing duty cycle perturbation quantities

Table 9. Simulated MPPT efficiencies using 10 kHz switching frequency for various duty cycle perturbation quantities

Irradiance (W/m^2)	**MPPT Efficiency (%)**			
	Δd = 0.001	**Δd = 0.005**	**Δd = 0.01**	**Varying Δd**
1000	96.29	96.29	96.29	96.29
800	97.06	97.06	97.06	97.06
600	97.12	97.12	97.12	97.12
400	96.31	96.31	96.31	96.31
200	91.97	91.97	98.76	99.76

Thus, the largest fixed duty cycle perturbation quantity of 0.01 and varying duty cycle perturbation quantity led the controller to track the MPP of the PV array more efficiently, especially at the lower irradiances, regardless of the DC-DC converter switching frequency.

3. Sampling Frequency

The effect of the MPPT sampling frequency on the MPPT efficiency of the controller was determined by simulating the PV power system using the P&O algorithm, 5 and 10 kHz switching frequency, fixed duty cycle perturbation quantity of 0.01 and varying duty cycle perturbation quantity, and 100, 200, and 400 Hz MPPT sampling frequencies.

First, the PV power system using the 5 kHz switching frequency and fixed duty cycle perturbation of 0.01 was simulated using the same irradiance steps and various controller sampling frequencies, Figure 24 and Table 10. At irradiances below 800 W/m^2 the MPPT efficiency of the controller increased as the sampling frequency increased. At the 1,000 and 800 W/m^2 irradiances, however, the fastest sampling frequency produced a significantly larger amount of noise than the slower sampling frequencies, reducing the overall efficiency of the control while also creating unwanted variations in the steady state power produced by the PV array.

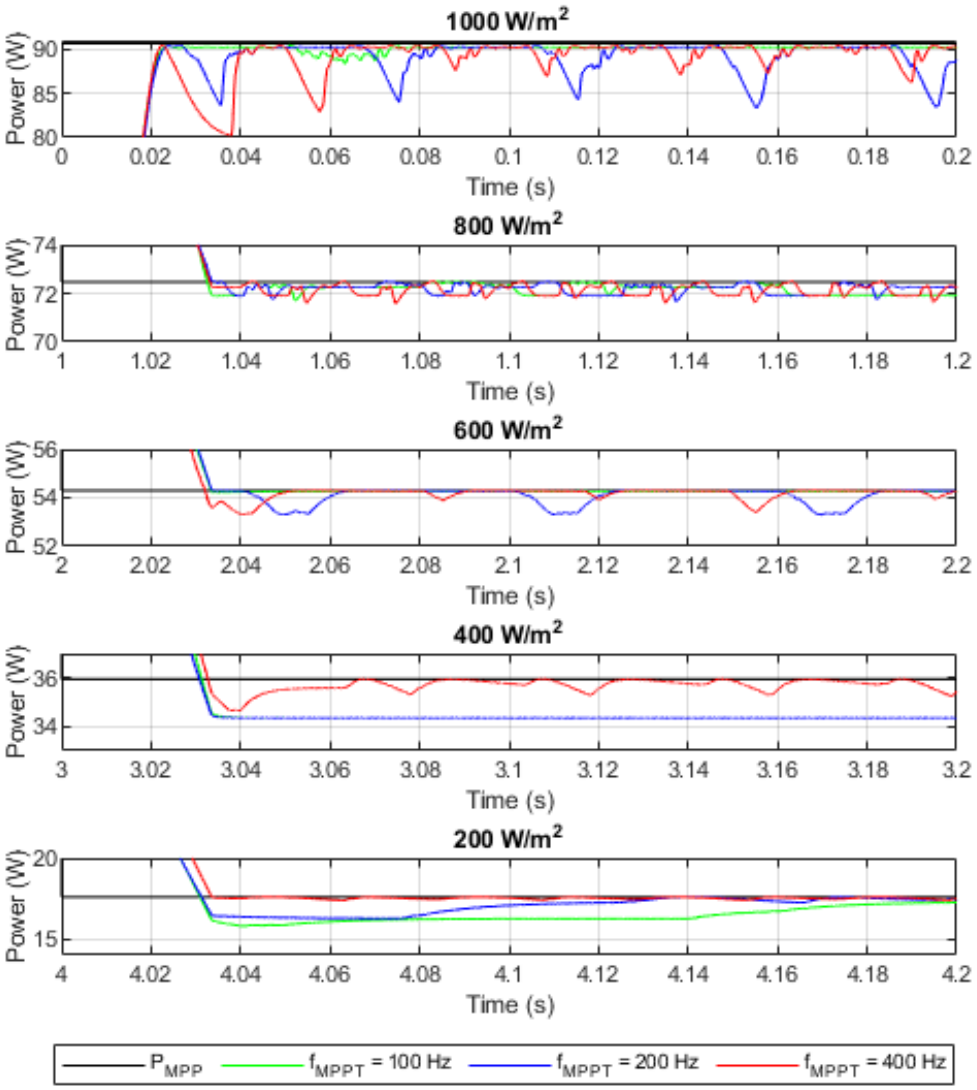

Figure 24. Simulated PV array power using 5 kHz switching frequency and fixed Δd of 0.01 comparing MPPT sampling frequencies

Table 10. Simulated MPPT efficiencies using 5 kHz switching frequency and fixed Δd of 0.01 comparing MPPT sampling frequencies

Irradiance (W/m^2)	**MPPT Efficiency (%)**		
	f_{MPPT} = 100 Hz	**f_{MPPT} = 200 Hz**	**f_{MPPT} = 400 Hz**
1000	99.53	99.25	98.62
800	99.21	99.59	99.55
600	99.94	99.63	99.82
400	95.55	95.55	99.49
200	98.99	99.28	99.62

Next, the PV system was simulated with the varying duty cycle perturbation quantity and the results are shown in Figure 25 and Table 11. The implementation of the varying duty cycle perturbation quantity produced the same efficiencies for both the 100 and 200 Hz sampling frequencies, with significant improvement seen at the 400 W/m^2 irradiance when compared to the efficiencies of the fixed duty cycle perturbation quantity. Although the magnitude and frequency of the power fluctuations at the 1,000 W/m^2 irradiance for the controller implementing the 400 Hz sampling frequency were significantly reduced, they were still present and resulted in a lower MPPT efficiency of the controller at the peak irradiance. The 400 Hz sampling frequency, did, however produce the highest efficiency at the lowest, 200 W/m^2, irradiance.

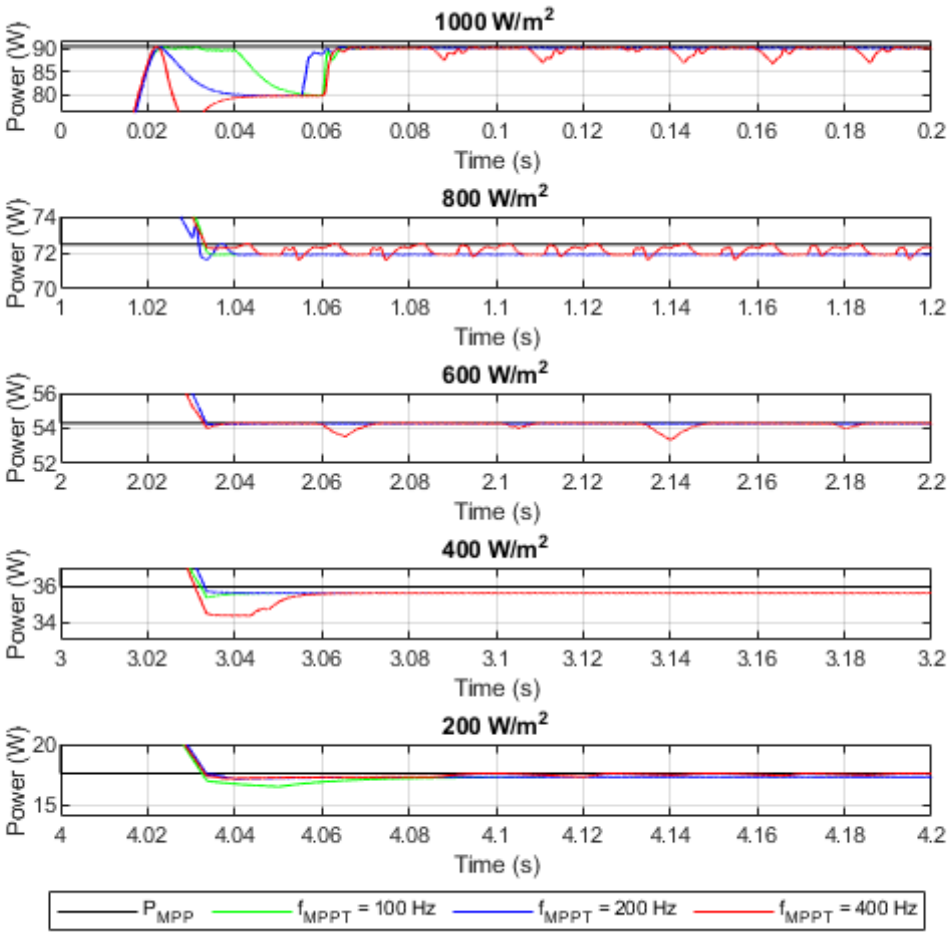

Figure 25. Simulated PV array power using 5 kHz switching frequency and varying Δd comparing MPPT sampling frequencies

Table 11. Simulated MPPT efficiencies using 5 kHz switching frequency and varying Δd comparing MPPT sampling frequencies

Irradiance (W/m^2)	**MPPT Efficiency (%)**		
	f_{MPPT} = 100 Hz	**f_{MPPT} = 200 Hz**	**f_{MPPT} = 400 Hz**
1000	99.53	99.53	98.83
800	99.21	99.21	99.55
600	99.94	99.94	99.82
400	99.01	99.01	99.01
200	98.33	98.33	99.61

The same procedure was followed for the system using the 10 kHz switching frequency. Interestingly, the controller achieved the same MPPT efficiencies noted in the previous section regardless of the MPPT sampling frequency used. Therefore, it was concluded that the MPPT sampling frequency for the system implementing the 10 kHz switching frequency did not affect the MPPT efficiency of the controller.

As shown in the previous results, the sampling frequency of the controller in conjunction with the duty cycle perturbation quantity, played a significant role in the MPPT efficiency of the system that implemented the 5 kHz switching frequency, particularly as the solar irradiance decreased. For both the fixed duty cycle perturbation quantity of 0.01 and varying duty cycle perturbation quantity, the 100 Hz sampling frequency resulted in the highest MPPT efficiencies for the span of irradiances simulated. When comparing these parameter configurations, varying the perturbation quantity led to a 3.5% higher efficiency at the 400 W/m^2, while the fixed quantity of 0.01 proved slightly better at the 200 W/m^2 irradiance.

Again, when comparing the PV power system with different converter switching frequencies, the system using the 5 kHz switching frequency produced higher MPPT efficiencies when compared to the 10 kHz switching frequency, which was not affected by the sampling frequency or duty cycle perturbation quantity. The cause for the poorer performance of the DC-DC converter using a 10 kHz switching frequency was the ratio of the simulation frequency to switching frequency. With the 10 kHz switching frequency, the ratio of simulation frequency to switching frequency was 10, whereas for the 5 kHz switching frequency it was 20. A larger ratio between these parameters is desired, which

was why the smaller switching frequency produced better simulated results. To verify this conclusion, the simulation was run using a 1 μs simulation time step. As expected, the MPPT efficiency of the controller implementing the 5 kHz switching frequency improved from the previous results using the 10 μs simulation time step. Furthermore, the 10 kHz switching frequency produced even higher MPPT efficiencies when compared to the 5 kHz switching frequency for the span of solar irradiances. However, since the time step for the simulator being used in the experimental set-up is restricted to 10 μs, the 5 kHz switching frequency will produce more efficient results when compared to the 10 kHz switching frequency.

4. MPPT Algorithm

The effect of the MPPT algorithm, P&O and INC, on the MPPT efficiency of the controller was determined by simulating the PV power system with the parameters identified by the results described in the previous sections. The final system included a 5 kHz DC-DC converter switching frequency, controller sampling frequency of 100 Hz, and a fixed duty cycle perturbation quantity of 0.01 or varying duty cycle perturbation quantity as previously described.

When comparing the PV array power using the fixed duty cycle perturbation quantity, in Figure 26, the INC algorithm induced larger, unwanted fluctuations in power at irradiances of 1,000, 600, and 400 W/m^2 when compared to the P&O algorithm. As noted in Table 12, these oscillations resulted in slightly smaller MPPT efficiencies at each irradiance step, with exception of the 400 W/m^2 irradiance. At this irradiance, the controller implementing the INC algorithm oscillated around the true MPP of the PV array, producing a higher efficiency, while the P&O algorithm locked on to a local, not true, MPP of the PV array.

Similar results were seen when comparing the PV array power using the varying duty cycle perturbation quantity, as shown in Figure 27. As depicted in Table 12, the power oscillations around the true MPP of the PV array observed using the INC algorithm produced approximately the same MPPT efficiencies as the P&O algorithm for the 800,

600, and 400 W/m^2 irradiances. However, the oscillations at the 1,000 W/m^2 produced a lower efficiency and a higher efficiency at the 200 W/m^2 irradiance.

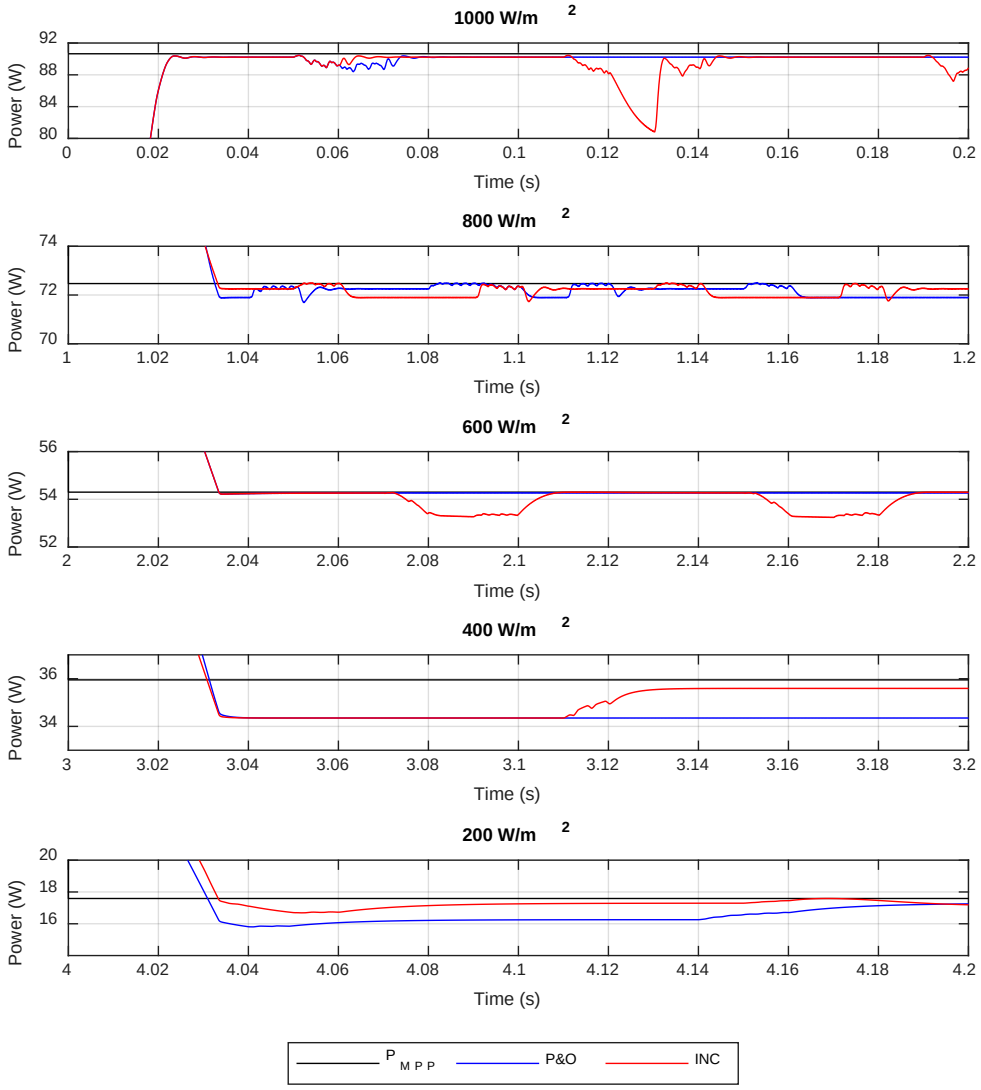

Figure 26. Simulated PV array power comparing MPPT algorithms with fixed Δd

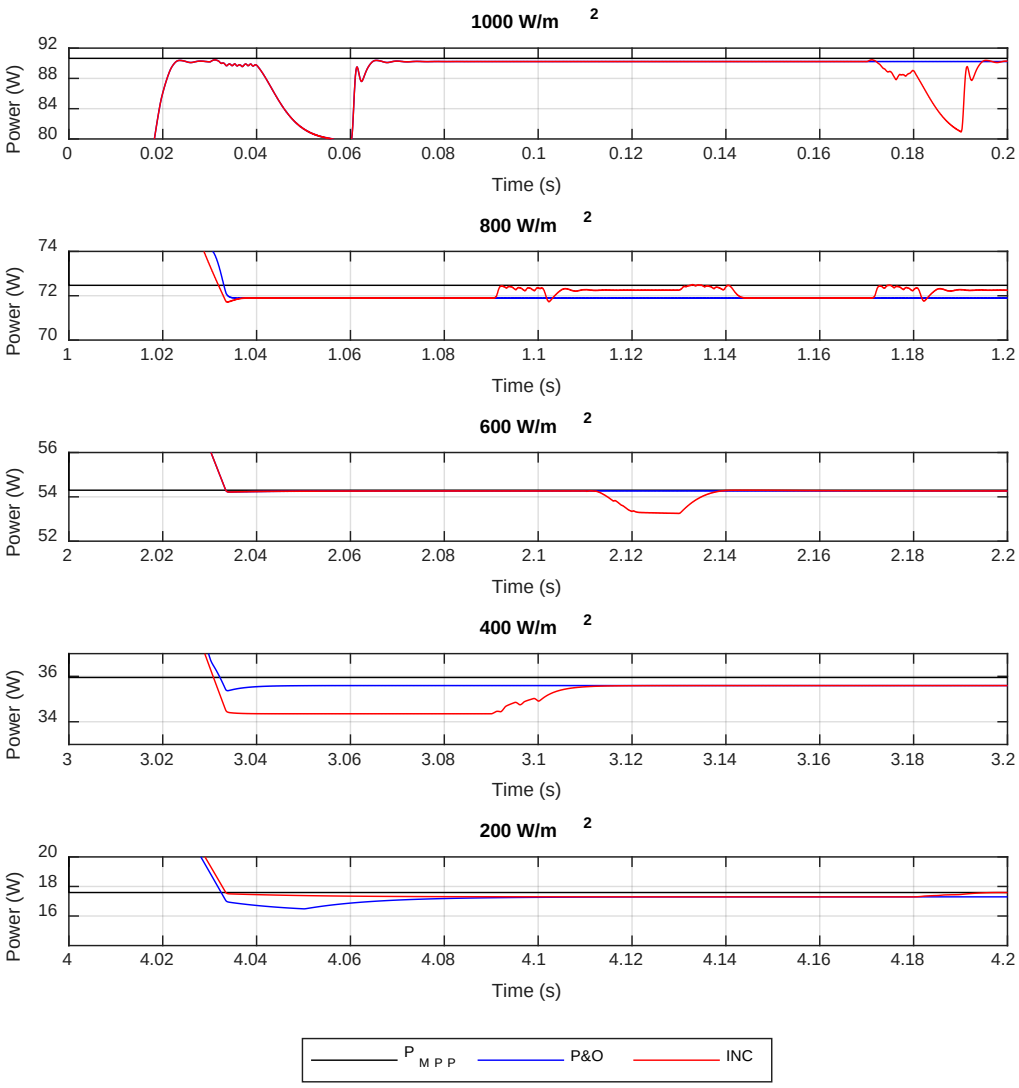

Figure 27. Simulated PV array power comparing MPPT algorithms with varying Δd

Table 12. Simulated MPPT efficiencies comparing MPPT algorithms

Irradiance (W/m^2)	**MPPT Efficiency (%)**			
	Mod. P&O (Fixed Δd)	**INC (Fixed Δd)**	**Mod. P&O (Varying Δd)**	**INC (Varying Δd)**
1000	99.53	98.31	99.53	98.87
800	99.21	99.59	99.21	99.59
600	99.94	99.41	99.94	99.64
400	95.55	98.68	99.01	98.92
200	98.99	98.99	98.33	98.96

As seen in the previous sections, it is important to note that the settling times for each algorithm and duty cycle perturbation quantity were identical, 0.0214 seconds. This reinforces the prior observation that the settling time produced by the MPPT controller for simulation of this particular PV power system is primarily affected by the switching frequency of the DC-DC converter.

In conclusion, the simulated P&O and INC algorithms proved successful in tracking the MPP of the PV array. The P&O algorithm outperformed the INC algorithm under constant solar irradiance conditions, creating minimal fluctuations in power after it locked on to a MPP after each irradiance step change. The steady state performance of the P&O algorithm also confirms that it fixed one of the main downsides of the basic P&O algorithm mentioned in the theory chapter, the power oscillation the basic algorithm produced around the MPP of the PV array. The INC algorithm, on the other hand, was more effective at locking on to the true MPP of the PV array during step changes in solar irradiance, confirming the theory discussed in the previous chapter.

THIS PAGE INTENTIONALLY LEFT BLANK

IV. EXPERIMENTAL TESTING AND RESULTS

This chapter discusses the experimental set-up of the PV power system used to evaluate the performance and efficiency of the MPPT controllers. Details of the practical implementation of the controllers in Opal-RT's eMEGASIM and RT-LAB software are also presented together with experimental results, and comparisons between the experimental and final simulated results from the previous chapter.

A. EXPERIMENTAL SET-UP

The PV power system shown in Figure 16 was built using a PV array, lead acid batteries, Semikron IGBT and gate driver, discrete components, and the Opal-RT RT simulator to implement the MPPT methods. The laboratory set-up is depicted in Figure 28.

Figure 28. PV power system experimental configuration

A Solartech SPM090P PV array, pictured in Figure 28, was used in the experimental set-up, provided the required voltage to charge a 24 V battery pack, and easily mounted to the side of the cart for experimentation purposes. The properties, power, voltage, current, and temperature coefficients, of the PV array are listed in Table 4 from the previous chapter.

The MPPT controller was designed in Opal-RT's RT-LAB using the eMEGASIM software and simulated in the OP4510 I/O system shown in Figure 29. The OP4510 system is a compact, fast, entry-level simulator designed for use in high-performance RCP and HIL simulations [25]. The user interface for the system was a personal computer, connected via an Ethernet cable, implementing the appropriate RT-LAB software and licenses. The computer interface was used to design, build, load, and run the MPPT controller on the OP4510 system, but it also provided a means of displaying and obtaining imported and exported data from the system using the MATLAB and Simulink workspace. Input analog signals to the OP4510 system included the PV array voltage and current, and the sole digital output was the PWM signal required to drive the DC-DC converter switch.

Figure 29. OP4510 simulator

A Semikron Semistack module (Figure 30), inductor, and smoothing capacitor were used to create the buck DC-DC converter used for the experimentation. The positive and negative terminals of the PV array were connected to the 1100 μF capacitor built in to the

Semikron Semistack module. A Semitrans 2 IGBT and diode, within the module, were used as the switch for the converter. To note, the module was designed for use in much higher voltage and current applications; therefore, it was not very efficient for low voltage applications due to the significant switching and conduction power losses. Since the purpose of this thesis was to focus on the controller, not overall efficiency of the PV power system, the IGBT served its purpose. The forward voltage drop across the IGBT at a temperature of 25°C typically measures 1.84 V but can reach as high as 2.29 V [26]. A PWM signal from the OP4510 I/O system drove the duty cycle and frequency of the IGBT. The output of the module was connected to the 232 μH inductor and the negative output was connected to the common ground of the DC load. A 1000 μF capacitor was implemented after the inductor to smooth the stepped-down voltage from the converter.

Figure 30. Semikron Semistack IGBT

As mentioned in the previous chapter, since PV arrays are intermittent sources of DC energy throughout an entire day, they are widely known for their use in charging energy storage devices; therefore, a battery was chosen as the DC load for this thesis. For the experiment, two 12 V, 17.2 amp-hour batteries were connected in series to obtain the desired voltage of 24 V.

Numerous sensors were used, as required, throughout the experimental configuration. The PV array voltage and current were measured using Tektronix probes and sent to the OP4510 I/O system for implementation into the MPPT controller. Since the probes reduce the magnitude of the measured signal by a predetermined amount, gain blocks with the appropriate values were added to the RT-Lab model of the system to ensure the true values of the voltage and current were used in the MPPT controller. The battery voltage was monitored using a standard multimeter to ensure it never exceeded normal steady state limits, causing an overvoltage. The PWM signal sent from the OP4510 I/O system to the Semikron Semistack IGBT was monitored using an oscilloscope to ensure the physical duty cycle matched the commanded one outputted from the MPPT controller. Lastly, the temperature and solar irradiance incident upon the PV array were measured using a Fluke Visual IR Thermometer and Amprobe Solar-100 Solar Power Meter, respectively.

B. RT-LAB MODEL

In order to build, load, and execute the original Simulink model of the PV power system in Opal-RT's RT-LAB software for HIL applications using the eMEGASIM solver, numerous modifications were required.

1. Subsystems

The first step in modifying the Simulink model for RT execution was grouping the components of the model into subsystems, distinguishing the computation elements from the GUI elements. GUI elements include those variables the user wishes to control or observe as the simulation is running. For example, these can include constant values, slider gains, displays, or scopes. Once all these GUI elements were consolidated, the subsystem received the required name "SC_GUI" as depicted in Figure 31. Computation elements are the mathematical manipulations within the model or the calculations. These elements are not controllable by the user as with the GUI elements. Once the computational elements were consolidated in a subsystem accordingly, the subsystem received the required name "SM_computation" as illustrated in Figure 32. If there were more than one computation subsystem, the follow-on subsystems would follow the naming format "SS_computation#," with # being the ordered number of the computational subsystem.

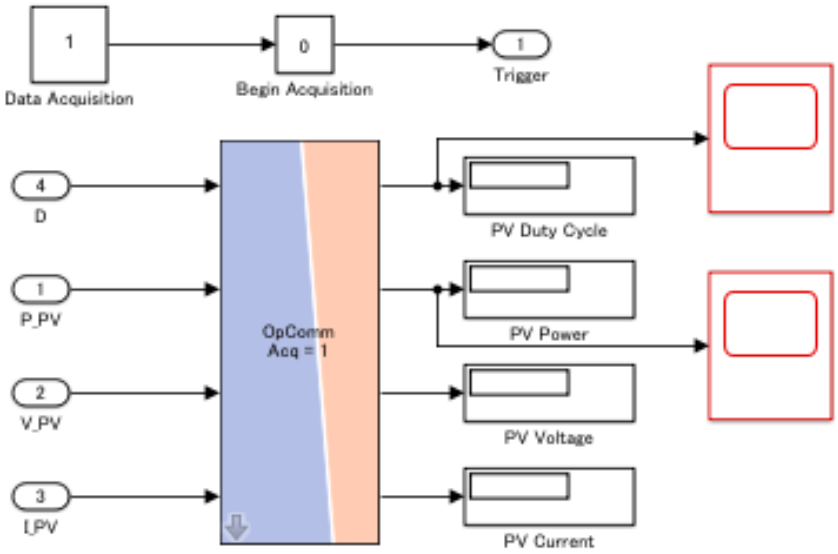

Figure 31. SC_GUI subsystem

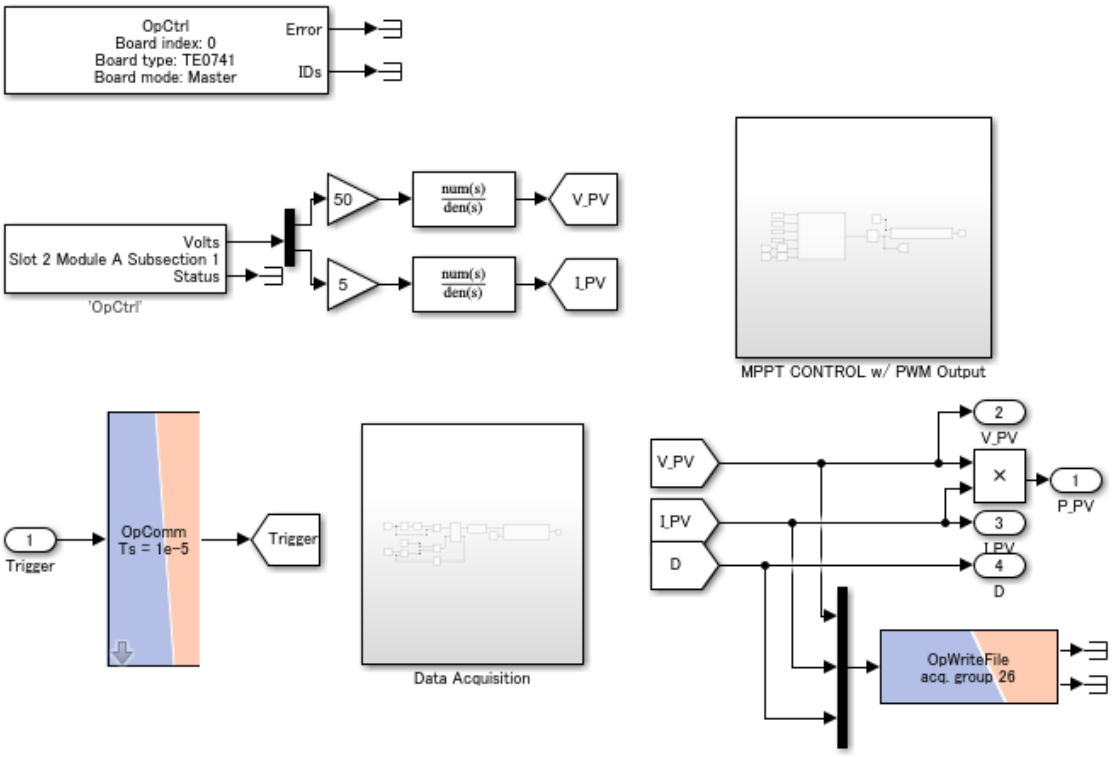

Figure 32. SM_computation subsystem

As a result, the top level of the modified Simulink model only displayed the subsystems and a “powergui” block, Figure 33. Each computation subsystem was assigned to one core on the RT target, or simulator, while the GUI subsystem was assigned to the host computer.

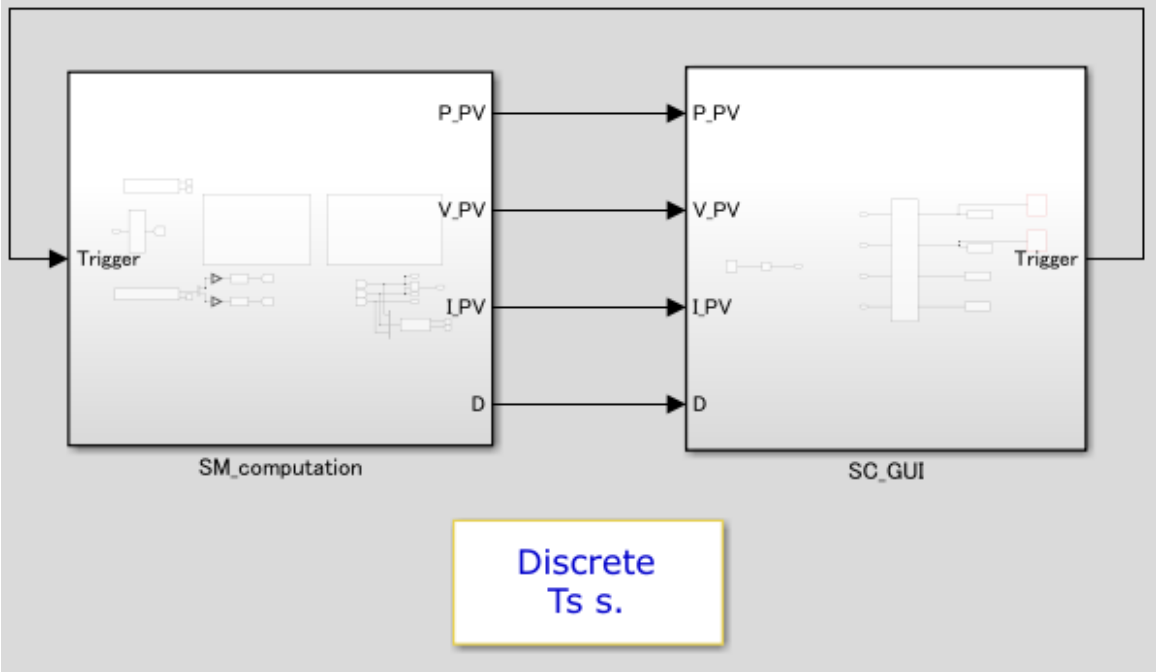

Figure 33. Modified Simulink model of PV power system with DC bus

2. I/O Interface

In order to use the OP4510 system as an RCP simulator, signals were required to be sent to and from the system. The voltage and current measurements of the PV array were read using an analog input card and Simulink control block, while the PWM signal for the DC-DC converter was sent using a digital output card and appropriate PWM Simulink control block. Both Simulink blocks were then controlled by an operational controller (OpCtrl) common mask block which controlled the programming of the analog and digital I/O cards, their initialization and selection of the hardware synchronization mode of the card, and enabled bind of the sending/receiving and I/O blocks to that specific card. The operational controller common mask block and analog input block are depicted

in Figure 32, and the PWM block is located in the MPPT CONTROL with PWM Output subsystem in the same figure. The I/O card used for both input and output signals was a TE0741 depicted in Figure 34.

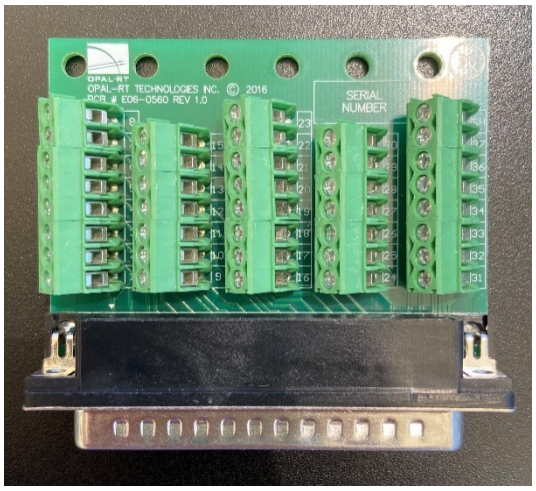

Figure 34. TE0741 I/O card

3. OpComm Blocks

The “OpComm” communication block, found in the Simulink block library provided by Opal-RT, is required for RT-LAB to “identify parameters required for communication between nodes in the hardware configuration” [27]. The inputs of all subsystems, including computational and GUI, must first go through an “OpComm” block before any operations can be done on the signals they are associated with [25]. The “OpComm” blocks are inserted after the subsystems are created and named. Each block can accept multiple scalar or vector inputs, however, they must all be within that one subsystem. The subsystems for the PV power system with “OpComm” blocks inserted are noted in Figure 31 and Figure 32.

4. Data Acquisition

Unlike Simulink, in which measurements or signals are sent to the workspace for comparison and analysis via a “To Workspace” block, the OP4510 simulator and RT-LAB requires the use of an “OpWriteFile” block with an appropriate trigger, implemented using

an “OpTrigger” block, to control when the data acquisition starts and stops. In order to compare the PV array powers from the simulated results with those from the experimental configuration, a logic algorithm was created to record the PV array voltage and current measurements and the duty cycle computed by the MPPT controller, as shown in Figure 35. When the experimentation was terminated using the RT-LAB software, the data was written into a .mat file and saved in the MATLAB workspace. The major restriction using the “OpWriteFile” block for data acquisition is the size restriction of the .mat file it produces, however, that was controlled by the decimation, or sampling, factor of the measurements in the parameters for the block.

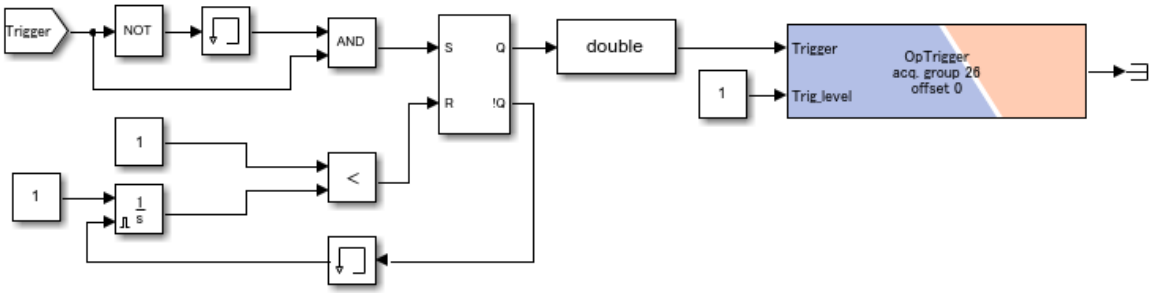

Figure 35. Data acquisition Simulink diagram

5. RT-LAB Simulation Parameters

a. Choice of Solver

Although variable-step solvers are easier to use, RT-LAB requires the use of a fixed-step solver for RT simulation applications since there is no means of knowing how long the next variable-step would last. The minimum size of this step is set by the software being used for simulation. For the eMEGASIM software being used in this thesis, the minimum step size is 10 μs, while for the eFPGASIM software, the minimum step size is 200 ns. An appropriate sample time must be chosen to ensure responses of the system are not missed, leading to less accurate results. For the experimental portion of this thesis, minimum step size for the eMEGASIM software, 10 μs, was used.

b. Target

Within the RT-LAB workspace, specific parameters must be adjusted prior to building, loading, and executing the controller being tested. The real-time simulation mode, located under execution properties, was adjusted from the standard, software synchronized, to hardware synchronized. This modification was required since the OP4510 system was being used for a HIL simulation implementing I/O blocks vice a SIL simulation. The model was also required to be assigned to the OP4510 using the assignation tab in the workspace. For the system to operate with the desired step of 10 μs, the extremely high performance block was also checked. Without adjusting these parameters, numerous error codes would be tricked when attempting to build the model in the RT-Lab workspace and load the model onto the OP4510 simulator.

C. EXPERIMENTAL RESULTS

Once the model was modified to operate in RT-LAB and on the OP4510 simulator as described beforehand, the MPPT controllers were implemented in the physical system. In the previous chapter, the efficiency of the controllers was computed for various levels of solar irradiance (1,000 W/m^2 to 200 W/m^2) and a constant PV array temperature of 25°C. For the experimental portion, the controllers were tested under various solar irradiances and temperatures, however, the environmental conditions did not match those of the previously simulated values. Therefore, the new irradiance values and temperatures from the experimental tests were inserted into the Simulink model from the previous chapter and re-simulated to provide power values comparable to those obtained with the experimental measurements.

First, the effect of the DC-DC converter switching frequency on the MPPT efficiency was revisited to determine if the simulation results were indeed correct or if they were a result of the size of the fix time-step used in the simulated model. As noted in Figure 20 and Table 7 of the previous chapter, a 5 kHz switching frequency produced larger MPPT controller efficiencies than both the 1 kHz and 10 kHz frequencies, specifically with higher solar irradiances. Intuitively, a larger switching frequency should produce a more efficient system when considering power losses across a converter, so the previous conclusion that

the 10 kHz switching frequency produced a smaller MPPT efficiency when compared to the 5 kHz switching frequency formed interesting results. To validate these results, the controller was tested using 5, 10, 12, and 15 kHz switching frequencies in the experimental set-up. The PV array power waveforms for a solar irradiance of 720 W/m^2 and a temperature of 53°C are illustrated in Figure 36 with mean values listed in Table 13. When comparing the waveforms, it was noted that each switching frequency produced similar power oscillations around a mean value; however, it also verified that the slowest switching frequency of 5 kHz enabled the PV array to produce more power than the larger frequencies. The average PV array power values listed in Table 13 verified this observation and the efficiencies of the simulation in the previous chapter. Therefore, with the controller operating at a 10 μs fixed time step (the lower limit of the eMEGASIM software being used), the 5 kHz DC-DC converter switching frequency enabled the system to more efficiently track the MPP of the PV array.

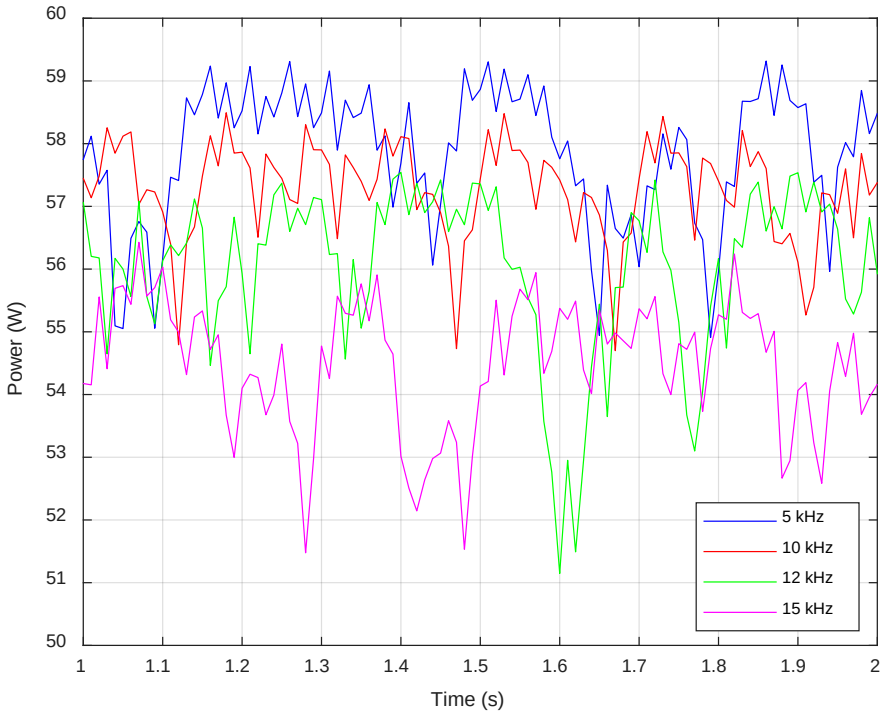

Figure 36. Experimental PV array power plots comparing DC-DC converter switching frequencies

Table 13. Experimental average PV array power measurements comparing DC-DC converter switching frequencies

DC-DC Converter Switching Frequency (kHz)	Average PV Array Power (W)
5	57.66
10	57.03
12	56.61
15	54.73

After confirming which DC-DC converter switching frequency enabled the controller to track the MPP of the PV most efficiently, the controller, implementing both MPPT algorithms and duty cycle perturbation methods, was tested in the experimental set-up. Results from each controller configuration were then compared to the simulated results from the previous chapter.

First, measurements were taken from the PV power system using the MPPT controller implementing the P&O algorithm with a fixed duty cycle perturbation quantity of 0.01, sampling frequency of 100 Hz, and DC-DC converter switching frequency of 5 kHz. As noted in Figure 37 and Table 14, the experimental model worked as designed, producing almost the same average powers as that of the simulated results. The largest difference between the experimental and simulated PV array powers of 1.55% occurred at the 180 W/m^2 irradiance.

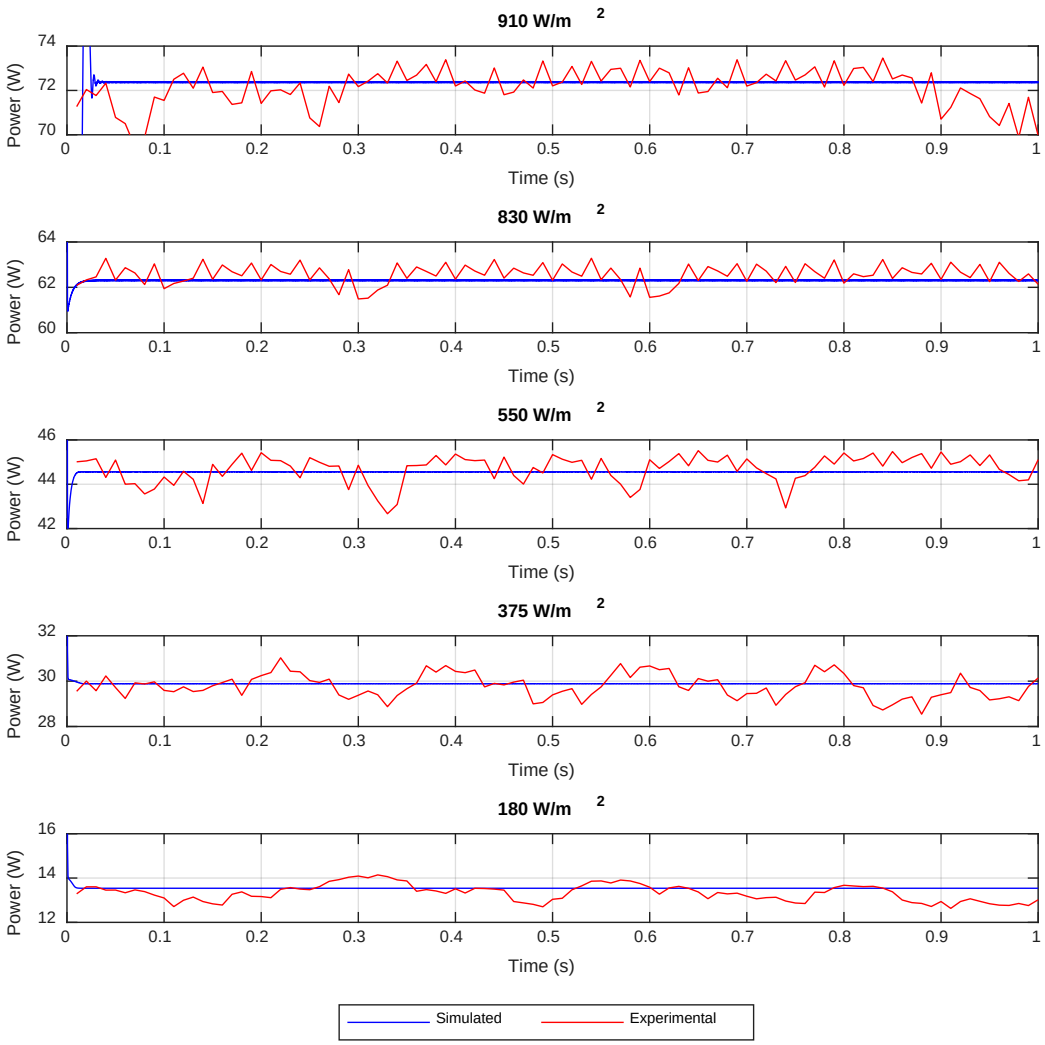

Figure 37. Simulated versus experimental PV array power measurements implementing the P&O MPPT algorithm with fixed Δd and PV array temperature of 48°C

Table 14. Simulated versus experimental average PV array power values using the P&O MPPT algorithm with fixed Δd and PV array temperature of 48°C

Irradiance (W/m^2)	**Average PV Array Power (W)**		
	Simulated	**Experimental**	**% Difference**
910	72.38	72.15	0.30
830	62.31	62.57	-0.41
550	44.56	44.69	-0.30
375	29.88	29.78	0.34
180	13.54	13.33	1.55

Next, measurements were taken from the PV power system using the MPPT controller implementing the P&O algorithm with the varying duty cycle perturbation quantity, sampling frequency of 100 Hz, and DC-DC converter switching frequency of 5 kHz. As noted in Figure 38 and Table 15, the experimental test showed the controller effectively tracked the MPPT at higher irradiances, but produced larger oscillations as the irradiance decreased. In a similar manner as the model implementing the fixed duty cycle perturbation quantity, the largest variance in average power when compared to the simulated results, 2.97%, occurred at the lowest irradiance, 260 W/m^2.

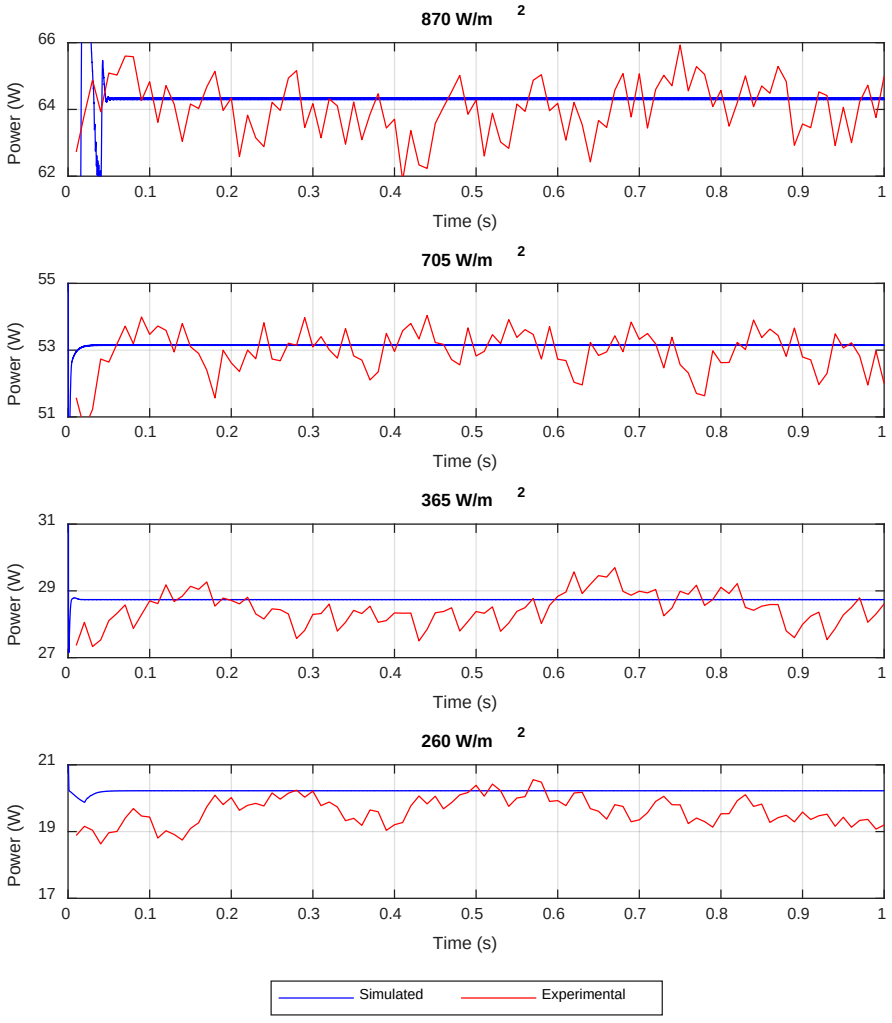

Figure 38. Simulated versus experimental PV array power plots implementing P&O MPPT algorithm with varying Δd and PV array temperature of 51°C

Table 15. Simulated versus experimental average PV array power values using the P&O MPPT algorithm with varying Δd and PV array temperature of 51°C

Irradiance (W/m^2)	**Average PV Array Power (W)**		
	Simulated	**Experimental**	**% Difference**
870	64.32	64.06	0.41
705	53.15	52.98	0.34
365	28.74	28.46	0.95
260	20.22	19.62	2.97

Then, measurements were taken from the PV power system using the MPPT controller implementing the INC algorithm with a fixed duty cycle perturbation quantity of 0.01, sampling frequency of 100 Hz, and DC-DC converter switching frequency of 5 kHz. As displayed in Figure 39 and Table 16, the experimental results confirmed the controller functioned in the experimental set-up as it did in the simulated model. To note, the largest difference in average powers, 1.09%, occurred at the lowest solar irradiance, 245 W/m^2.

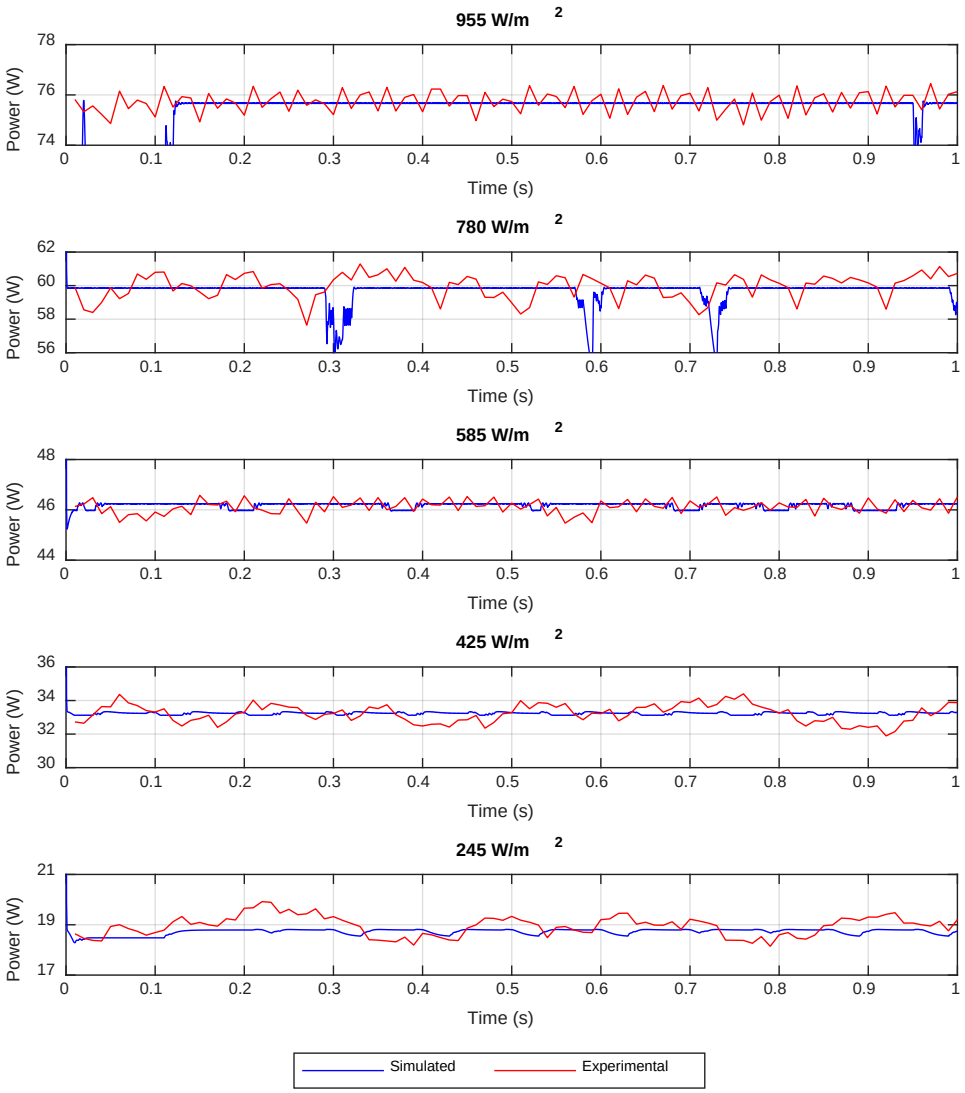

Figure 39. Simulated versus experimental PV array power plots implementing INC MPPT algorithm with fixed Δd and PV array temperature of 53°C

Table 16. Simulated versus experimental average PV array power values using the INC MPPT algorithm with fixed Δd and PV array temperature of 53°C

Irradiance (W/m^2)	Average PV Array Power (W)		
	Simulated	Experimental	% Difference
955	75.64	75.73	-0.11
780	59.63	59.96	-0.55
585	46.18	46.12	0.13
425	33.24	33.23	0.03
245	18.75	18.95	-1.09

Lastly, measurements were taken from the PV power system using the MPPT controller implementing the INC algorithm with a varying duty cycle perturbation quantity, sampling frequency of 100 Hz, and DC-DC converter switching frequency of 5 kHz. As presented in Figure 40 and Table 17, the experimental test verified the controller worked as designed and simulated. As with the INC algorithm implementing the fixed duty cycle perturbation quantity, the largest variance in average power values, 1.23%, occurred at the lowest irradiance, 180 W/m^2.

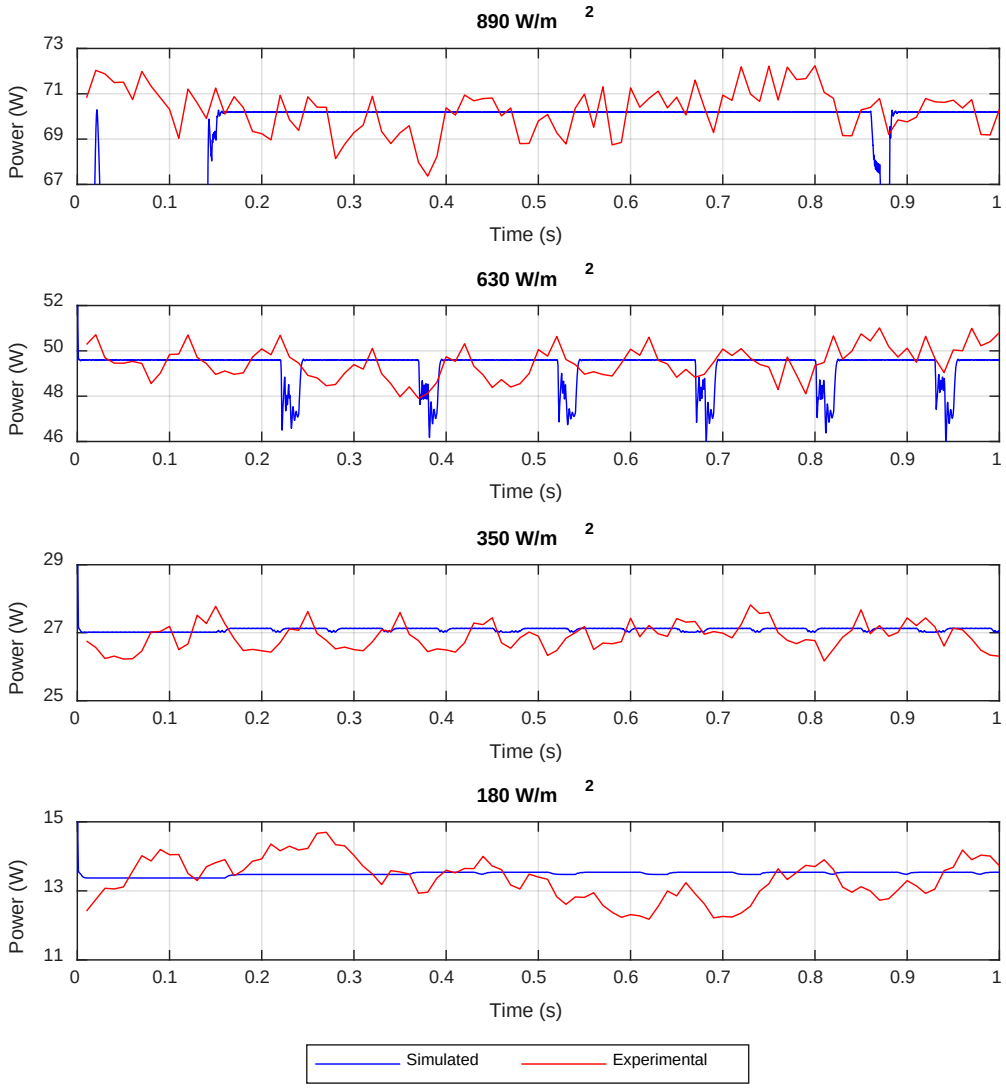

Figure 40. Simulated versus experimental PV array power plots implementing INC MPPT algorithm with varying Δd and PV array temperature of 54°C

Table 17. Simulated versus experimental average PV array power values using the INC MPPT algorithm with varying Δd and PV array temperature of 54°C

Irradiance (W/m^2)	Average PV Array Power (W)		
	Simulated	Experimental	% Difference
890	70.05	70.28	-0.32
630	49.31	49.49	-0.37
350	27.10	26.89	0.78
180	13.52	13.36	1.23

Some important observations were made when comparing these results. Foremost, when comparing the power at the various irradiances, it was noted that the experimental measurements contained a great deal of oscillation around the mean powers whereas the simulated values remained somewhat constant. For the majority of the irradiances, this power variation was directly related to the magnitude of the solar irradiance incident upon the PV array. In the simulation, the irradiance was held constant between each step change. In the physical system, however, the irradiance from the sun never remained constant, but rather fluctuated around some mean value. This dynamic solar irradiance also effects the efficiency of MPPT controller due to the tolerances in each algorithm. For the P&O algorithm, the duty cycle only remained the same as the previous control step when the change in power between steps was less than 0.001 W. For the INC algorithm, the previous duty cycle was only used when there wasn't a change in voltage and current from the previous control step, or if there wasn't a change in voltage and the incremental conductance equaled the instantaneous conductance. For the smaller irradiances, particularly with the algorithms implementing the varying duty cycle perturbation quantity, noise seemed to play a factor in the efficiency of the controller. Considering the environmental conditions under which the measurements were taken, the voltage of the PV array at the lower irradiances hardly resulted in the requirement of a step-down converter to charge the 24 V battery pack when factoring in losses across the IGBT. Additional noise in the system caused the controller to update the duty cycle incorrectly, which, in the end, led to the larger fluctuations in power around the simulated results.

The second observation, as discussed in the theory chapter, was the effect of PV array temperature on power output. For example, when comparing the experimental power at an irradiance of 910 W/m^2 and temperature of 48°C and the theoretical power at an irradiance of 910 W/m^2 and temperature of 25°C, the average experimental power was 10.2 W or 12.36% less than the theoretical results. The 23°C increase in the temperature of the PV array significantly impacted the output power. This decrease in power was noted throughout the span of irradiances under which measurements were conducted.

The last observation was the overall performance of the different MPPT algorithms. When comparing the control algorithms implementing the fixed duty cycle perturbation quantity of 0.01, the INC algorithm produced slightly less fluctuations in power around the MPP of the PV array for the span of irradiances tested. Although the conventional P&O algorithm was slightly modified to reduce these power variations, which proved more efficient in simulation when compared to the INC algorithm, the experimental tests confirmed the theory that the INC algorithm tracks the MPP of the PV array more effectively under steady state solar irradiance conditions. The controllers implementing the varying duty cycle perturbation quantity, on the other hand, seemed to produce the same power fluctuations for each of solar irradiance with exception of the lowest. At the lower irradiances, the INC algorithm using the varying duty cycle perturbation quantity tracked the MPP of the PV array slightly more efficiently.

V. CONCLUSIONS AND RECOMMENDATIONS

This chapter summarizes the results from simulation and experimental validation of a stand-alone PV power system with different MPPT controllers implemented on a digital platform. Furthermore, some recommendations for future work with PV power systems and other microgrid applications are discussed.

A. CONCLUSIONS

The research presented in this thesis successfully explored the application, design, and efficiency of a digital MPPT controller using a step-down DC-DC converter in a stand-alone PV power system through software simulation and experimental testing. The main observations and lessons learned are detailed in the following sections.

1. Maximum Power Point Tracking Algorithm Comparison and Parameter Optimization

In theory, both MPPT algorithms have their advantages and disadvantages. The conventional P&O algorithm is simple and easier to implement in a digital controller, but it causes the PV array to fluctuate about, rather than operate at, the MPP during constant solar irradiance conditions. The INC algorithm is more complex and requires more calculations during each control step, however it is able to stabilize at the MPP of the PV array during constant solar irradiance conditions. The P&O algorithm presented in this thesis combined the simplicity of the conventional P&O algorithm with the stability of the INC algorithm.

In simulation and experimental testing, both the P&O and INC control algorithms effectively and efficiently tracked the MPP of the PV array. The efficiency for each algorithm was significantly affected by the DC-DC converter switching frequency, the duty cycle perturbation quantity, and sampling frequency of the digital controller. For the particular PV power system discussed in this thesis, simulation and experimental testing confirmed that a 5 kHz converter switching frequency and 100 Hz controller sampling frequency resulted in the highest MPPT efficiency for both algorithms, regardless of the duty cycle perturbation quantity implemented. A varying duty cycle perturbation quantity

produced higher efficiencies in simulation; however, a fixed duty cycle perturbation quantity of 0.01 produced higher efficiencies and less power fluctuations in experimental testing, specifically at lower levels of solar irradiance. In simulation, the P&O algorithm implementing a varying duty cycle perturbation quantity actually locked on to the MPP of the PV array vice fluctuating about it and outperformed the INC algorithm. In experimental testing, however, the INC algorithm using a fixed and varying duty cycle perturbation quantity produced slightly better results. During simulation and experimental testing, it was also noted that each algorithm was capable of tracking a local MPP vice the true MPP of the PV array.

2. Environmental Effects on PV Array Power Production

When implementing PV arrays as a DC power generator in a microgrid, careful consideration must be taken into which environment the system will be employed. The solar radiation incident upon the PV array and the temperature at which it will operate significantly affect the power output. The dependence on high values of solar irradiance and low operating temperatures also reinforces the fact that PV arrays are not a reliable source of power when used as the sole generating component in a microgrid, but rather assist other power generating components during times of higher demand or in charging energy storage devices such as batteries.

3. Benefits of Rapid Control Prototyping using a Real-Time, Hardware-in-the-Loop Simulator

The use of a RT simulator enabled the testing of the MPPT controller in a physical microgrid with a PV array as power source, something software simulation alone does not provide. Unlike programming standard micro-computers for their use in control applications, the model and parameters of the controller can be adjusted immediately within the RT simulator, providing faster feedback on the capabilities and effectiveness of the controller in its designed use. A RT simulator also provides a means of efficient data collection and analysis, reducing the requirement for older measurement devices and data processing methods.

B. FUTURE WORK

This sections briefly discusses recommendations for future work implementing the RT, HIL simulator in microgrid analysis.

1. Overall Efficiency of the PV Power System

The main objective of this thesis was to study the efficiency of the MPPT controller for use with a commercial off-the-shelf PV array, not the overall efficiency of the entire system including the DC-DC converter. Therefore, the step-down DC-DC converter was not engineered to reduce power losses, but rather it was built from readily available inductors, capacitors, and a very large IGBT with a much higher voltage and current rating than required. Reducing the size of the energy storage devices and acquiring a faster transistor, such as a metal-oxide semiconductor field-effect transistor (MOSFET), could minimize the conduction and switching losses associated with these components, improving the overall efficiency of the system.

2. Different Configurations of PV Arrays using RT Simulator

This thesis studied the efficiency of a controller tracking the MPP of a single PV array; however, solar energy is rarely harvested using one array. Rather a configuration of PV arrays in series, parallel, or both is implemented to increase the overall power output of the system to a practical value. Follow on experiments can study the efficiency of a controller in tracking the MPP of multiple PV arrays connected in series, parallel, and both. This configuration will facilitate studies on the effects of partial shading and the impact on the MPPT efficiency of the entire PV array power conditioning system. It will also provide insight as to which controller configuration is most effective and feasible when trying to achieve the highest MPPT efficiency for the group of arrays, i.e., one per array, one per string, or one for all of the arrays in series and parallel.

3. Expand the Microgrid to Incorporate More Power Generation and Storage Components and a Single or Three-Phase AC Bus

The microgrid studied in this thesis incorporated a PV array as a DC power source, MPPT controller, and batteries as an energy storage device and DC load. Future work can

explore the introduction of an AC, single or three-phase, bus and the integration of more power generation and storage components to include diesel generators, wind and water turbines, and capacitors. The ability to connect the microgrid to an AC grid would also facilitate more research opportunities. An analysis on transitions to and from grid connected mode can help analyze and reduce the significant fluctuations in voltage, current, and frequency caused by an unintentional islanding event, improving the resilience of the microgrid.

LIST OF REFERENCES

[1] Department of the Navy, *Commandant's Planning Guidance: 38th Commandant of the Marine Corps*. Washington, DC, USA, 2019. [Online]. Available: https://www.hqmc.marines.mil/Portals/142/Docs/%2038th%20Commandant%27s%20Planning%20Guidance_2019.pdf?ver=2019-07-16-200152-700.

[2] *Littoral Operations in a Contested Environment.* Department of the Navy. Washington, DC, 2017.

[3] Concepts and Programs, United States Marine Corps, "Mobile amphibious assault fuel distribution." Accessed May 10, 2020. [Online]. Available: https://www.candp.marines.mil/Programs/Focus-Area-4-Modernization-Technology/Part-8-Expeditionary-Energy/Mobile-Amphibious-Assault-Fuel-Distribution/.

[4] Headquarters, United States Marine Corps, "Expeditionary Energy Concepts (E2C) 2016." Accessed May 10, 2020. [Online]. Available: https://www.hqmc.marines.mil/Portals/160/Docs/160825_Factsheet_E2C2016.pdf?ver=2016-08-25-112509-927.

[5] Solar Portable Alternative Communications Energy System (SPACES). (n.d.). IRIS Technology Corporation, Irvine, CA. Accessed May 10, 2020. [Online]. Available: https://www.iristechnology.com/wp-content/uploads/2015/05/Man-Portable-Power-System.pdf.

[6] Ground Renewable Expeditionary Energy Network System (GREENS). (n.d.). UEC Electronics, LLC, Hanahan, SC. Accessed May 10, 2020. [Online]. Available: https://www.uec-electronics.com//wp-content/themes/uec/images/downloads/GREENS-Spec-Sheet.pdf.

[7] DON Innovation, "2015 SECNAV innovation award honorable mention: Marine Corps Expeditionary Energy Office (E2O)," NavalX, May 20, 2016. [Online]. Available: https://www.secnav.navy.mil/innovation/Pages/2016/05/MarineCorpsE2O.aspx.

[8] A. Selko, "Expansion management: aerospace sector flying high in Charleston, SC," Industry Week, September 6, 2014. [Online]. Available: https://www.industryweek.com/expansion-management/article/21963709/expansion-management-aerospace-sector-flying-high-in-charleston-sc.

[9] T. Esram and P. Chapman, "Comparison of photovoltaic array maximum power point tracking techniques," *IEEE Trans. Energy Convers.*, vol. 22, no. 2, pp. 439–449, Jun. 2007.

[10] A. Belkaid, I. Colak, K. Kayisli, R. Bayindir, “Design and Implementation of a Cuk Converter Controlled by a Direct Duty Cycle INC-MPPT in PV Battery System,” *Int. J. of Smart Grid*, vol. 3, no. 1, pp. 19–25, Mar. 2019.

[11] B. Panigrahi and P. Thakura, “Implementation of Cuk Converter with MPPT,” in *3rd Int. Conf. on Advances in Elect., Electron., Inform., Commun., and Bio-Informatics*, Chennai, India, Feb. 2017.

[12] S. Saravanan and N. Ramesh Babu, “Performance Analysis of Boost & Cuk Converter in MPPT Based PV System,” in *Int. Conf. on Circuit, Power, and Computing Technol.*, Nagercoil, India, Mar. 2015.

[13] J. S. Topping, “Maximum power point tracking of a photovoltaic system utilizing an interleaved boost converter,” M.S. thesis, Dept. Elect. and Comp. Eng., Naval Postgrad. School, Monterey, CA, 2015.

[14] T. D. Bailey, “Modeling and implementing a digitally embedded maximum power point tracking algorithm and a series-loaded resonant DC-DC converter to integrate a photovoltaic array with a micro-grid,” M.S. Thesis, Dept. Elect. and Comp. Eng., Naval Postgrad. School, Monterey, CA, 2014.

[15] M. Z. C. Wanik, A. Bousselham, A. Elrayyah, “Real-time simulation modeling for PV-battery based microgrid system,” in *2016 IEEE Int. Conf. on Power Syst. Technol.*, Sep. 2016.

[16] J. Khazaei, L. Piyasinghe, Z. Miao, and L. Fan, “Real-time digital simulation modeling of single-phase PV in RT-LAB,” in *2014 IEEE PES General Meeting | Conf. & Exposition*, National Harbor, MD, Jul. 2014, pp. 1–5.

[17] Saroja K. Sahoo, A. K. Sinha, N. K. Kishore, “Modeling and real-time simulation of an AC microgrid with solar photovoltaic system,” in *IEEE India Conf.*, New Delhi, India, Dec. 2015, pp. 1–6.

[18] O. Crăciun, A. Florescu, S. Bacha, I. Munteanu and A. I. Bratcu, “Hardware-in-the-loop testing of PV control systems using RT-Lab simulator,” in *Proc. of The 14th Int. Power Electron. and Motion Control Conf.*, Ohrid, Sep. 2010, pp. S2-1-S2-6.

[19] G. Dilee, S. N. Singh, “Selection of non-isolated DC-DC converters for solar photovoltaic system,” *Renewable and Sustainable Energy Rev.*, vol. 76 pp. 1230–1247, 2017.

[20] N. Mohan, T. M. Undeland, and W. P. Robbins, *Power Electronics: Converters, Applications, and Design*, 3rd ed. Hoboken, NJ: John Wiley & Sons, Inc., 2003.

[21] I. V. Banu, R. Beniugă and M. Istrate, “Comparative analysis of the perturb-and-observe and incremental conductance MPPT methods,” in *2013 8th Int. Symp. on Advanced Topics in Elect. Eng.*, Bucharest, Romania, May 2013, pp. 1–4.

[22] D. Jie, Z. Chun-jiang and L. Yan-bang, “Comparison of duty ratio perturbation & observation and reference voltage perturbation & observation methods applied in MPPT,” in *Proc. of The 7th Int. Power Electron. and Motion Control Conf.*, Harbin, China, June 2012, pp. 1358–1362.

[23] Simscape. MathWorks, Natick, MA. Accessed February 6, 2020. [Online]. Available: https://www.mathworks.com/products/simscape.html.

[24] W-Series 90 W PV Module SPM090P-WP-F. Solartech Power, Inc., Ontario, Canada. Accessed May 28, 2020. [Online]. Available: https://www.solartechpower.com/images/Wseies/SPM090P-WP-F.pdf.

[25] OP4510 simulator. Opal-RT Technologies, Montreal, Canada. Accessed March 12, 2020. [Online]. Available: https://www.opal-rt.com/simulator-platform-op4510/.

[26] Semikron, *SKM50GB12V Semitrans 2*, 2016. [Online]. Available: https://www.semikron.com/products/product-classes/igbt-modules/detail/skm50gb12v-22892003.html.

[27] *RT-Lab Solo*, ver. 2.11, McGill Univ. Intell. Automat. Lab, Montreal, Canada, 2003. [Online]. Available: http://www.cim.mcgill.ca/~ialab/members/usefuldoc/RTLab_Instructions_v2.11.pdf.

THIS PAGE INTENTIONALLY LEFT BLANK

INITIAL DISTRIBUTION LIST

1. Defense Technical Information Center
   Ft. Belvoir, Virginia

2. Dudley Knox Library
   Naval Postgraduate School
   Monterey, California